2012-11-19

Laboratory Investigation of Polymer-flooding, ASP-flooding, and Foam-flooding in Heavy Oil System

Su, Shi

UNIVERSITY OF CALGARY

Laboratory Investigation of Polymer-flooding, ASP-flooding, and Foam-flooding in Heavy Oil System

by

Shi Su

A THESIS

SUBMITTED TO THE FACULTY OF GRADUATE STUDIES

IN PARTIAL FULFILMENT OF THE REQUIREMENTS FOR THE

DEGREE OF MASTER OF SCIENCE

DEPARTMENT OF CHEMICAL AND PETROLEUM ENGINEERING

CALGARY, ALBERTA

November, 2012

UNIVERSITY OF CALGARY

FACULTY OF GRADUATE STUDIES

The undersigned certify that they have read, and recommend to the Faculty of Graduate Studies for acceptance, a thesis entitled "Laboratory Investigation of Polymer-flooding, ASP-flooding, and Foam-flooding in Heavy Oil System" submitted by Shi Su in partial fulfilment of the requirements of the degree of Master of Science.

_____

Supervisor, [FULL NAME AND DEPARTMENT]

_____

[FULL NAME AND DEPARTMENT]

_____

[FULL NAME AND DEPARTMENT]

_____

[FULL NAME AND DEPARTMENT]

_____

DOCTORAL STUDENTS ONLY External Examiner (or External Reader), [FULL NAME AND INSTITUTION]

_____

Date

Abstract

It is widely accepted that thermal methods have become the most effective techniques for Alberta heavy oil reservoirs. However, thermal techniques cannot be applied to many reservoirs, such as deep reservoir or reservoir with thin pay because heat losses will be too severe. Water flooding is an alternative but it can only achieve a very low oil recovery due to severe viscous fingering. Hence, research into other non-thermal recovery methods is necessary.

This thesis presents a laboratory-scale investigation of heavy oil recovery by polymer flooding, ASP (alkali-Surfactant-Polymer) flooding and ASP-foam flooding. The production mechanisms involved in heavy oil chemical flooding and foam-flooding were studied. Several sandpacks saturated with the heavy oil were first waterflooded. Then either polymer, ASP or ASP-foam flooding was conducted. The recovery performance of these displacements was evaluated and compared. The effect of injection rates was also studied. ASP flooding at low injection rate achieved the highest oil recovery. Under the high injection rate, polymer flooding, ASP flooding and, ASP-foam flooding recovered similar amounts of oil. Oil recoveries of polymer-flooding were insensitive to injection rate. Besides, ASP foam flooding of a water saturated core (oil-free) was also conducted. A comparison between the displacements of the oil-free core with that of the previous displacement tests suggested that foam stability was destroyed in the presence of heavy oil.

Acknowledgements

I am grateful for the help and guidance of my supervisor, Dr. Apostolos Kantzas, whose kindness, inspiration and encouragement made the preparation of my thesis possible. Under his supervision, I have gained an invaluable experience and for that I am forever in his debt. I would like to highlight my sincere appreciation to my research mentor Dr. Jon Bryan. His encouragement, patience, motivation, supervision and his many words of advice during the entire research period at the University of Calgary are paramount to my study and research.

I would also like to thank Dr. Harvey Yarranton, for providing me with a tensiometer, which is extremely helpful to my thesis. My special thanks to Dr. George Hirasaki (Department of Chemical and Biomolecular Engineering, Rice University), whose invaluable suggestions greatly improved my experiments.

My gratitude is also expressed to all my friends. They have all contributed to providing me with the most pleasant and enjoyable conditions in Calgary, favourable to the development of productive research.

Finally, I would like to express my deep appreciation to my parents, Yanchun Su and Zhifeng Shi, for their love, support, and understanding, without which I could not have possibly finished this project.

Dedication

To my parents (Yanchun Su and Zhifeng Shi).

For their unconditional love and giving.

Table of Contents

List of Tables

List of Figures and Illustrations

List of Symbols, Abbreviations and Nomenclature

Symbol	Definition
API gravity	The American Petroleum Institute gravity
OOIP	Original Oil In Place
IFT	Interfacial Tension
ASP flooding	Alkali Surfactant Polymer flooding
ASPF flooding	Alkali Surfactant Polymer Foam flooding
MMbpd	Million Barrels of Oil Per Day
PPM	Percent per Million
N	Capillary Number
μ	Viscosity
σ	Interfacial Tension
v	Darcy velocity of the fluid
CT	Computed Tomography
EOR	Enhanced Oil Recovery
ρ_h	The Density of Heavy Phase
ρ_d	The Density of Light Phase,
ω	The Rotational Velocity
D	The Measured Drop Diameter
L	Length
DI water	Deionized Water
F_w	Wilhelmy Force,
θ	Contact Angle between Liquid and Platinum Plate
α	Linear Attenuation Coefficient
Io	Incident X-ray intensity
I	Measured Intensity after Penetrating Sample
x	Sample Thickness
$\emptyset$	Porosity
ρ_g	Grain Density
ρ_{gas}	Gas Density
ρ_m	Measured Density
ρ_f	Fluid Density
f_g	Gas Saturation
Q	Volumetric Flow Rate
k	Permeability
Δp	Pressure Drop
μ	Fluid Viscosity
γ_{eq}	Shear Rate
A	Cross Sectional Area
p_1	Atmosphere Pressure
w_1	Water Mass
p_2	Gauge Pressure
ρ_w	Water Density
V'	Dead Volume

s_{wi}	Initial Water Saturation
μ_p	Effective Polymer Viscosity
μ_o	Oil Viscosity
ρ_o	Oil Density
k_o	Oil Permeability
k_w	Water Permeability
ρ_f	Fluid Density
ρ_l	Liquid Density
s_w	Water Saturation
k_{por}	Polymer Permeability at the End of Polymer Flooding
k_{wor}	Water Permeability at the End of Water Flooding
k_{oiw}	Oil Permeability at the End of Oil Flooding
Δp_o	Pressure Drop at the End of Oil Flooding
Δp_w	Pressure Drop at the End of Water Flooding
Δp_p	Pressure Drop at the End of Polymer Flooding

Chapter One: INTRODUCTION

Heavy oil has become an attractive resource, since conventional oil is reaching the maximum production and the world oil demand continues to grow. Dusseault (2002) reported that after 2015, contributions of the heavy oil to total oil production would reach 0.64 million cubic meters per day and keep this relatively high level for several years. The heavy oil resources of the world total about 1.6 trillion cubic meters, nearly three times the conventional oil-in-place in the world (Salama et al, 2005). The Canadian heavy oil and oil sand deposits comprise the largest known petroleum accumulation in the world, with over 400 10^9 m^3 OOIP. However, recovery of heavy oil from the reservoir is still a difficult task due to its low API gravities and high viscosity.

Canada heavy oil and bitumen resources are some of the largest in the world. Waterflooding is a recognized technique in many Canadian heavy oil reservoirs, where the oil has some, albeit limited, mobility under reservoir conditions. In certain reservoirs, such as thin pay systems (e.g 5m reservoir thickness) or deep reservoirs, only non-thermal technology methods can be applied. Within these reservoirs waterfloods are highly inefficient due to adverse mobility ratio and viscous fingering, and more effective non-thermal EOR methods are required in order to accelerate and enhance oil production.

One option is polymer flooding which has been shown to improve the mobility ratio and recover additional heavy oil after water flooding (Green et al, 1998). Adding alkali and surfactant into polymer solution (ASP) can improve the oil displacement of the process because the surfactant generates ultra low IFT and the alkali formed extra in-situ co-surfactants (Krumrine et al., 1982). Although the displacement mechanisms of ASP flood are similar to polymer flood, ASP flooding is a much newer technology, is more complex and costly, and is not technically well developed for heavy oil reservoirs. Laboratory tests have shown that adding gas to the ASP fluid to form ASP foam (ASPF) provided ultra-low IFT and also low mobility (Wang et al, 2001). These characteristics may allow ASPF to save more cost than ASP flooding to reach the same oil recovery.

The objective of this study is to investigate the oil recovery mechanisms of polymer flooding, ASP flooding and ASPF flooding as EOR methods for heavy oil from Western Canada reservoirs. Previous work in this area focused on the specific sizes of the injected chemical slug and it was challenging to distinguish the difference between polymer, ASP, and foam displacements. In this thesis, post-waterflood displacements were conducted for each fluid until the water cut reached 100%. The oil recovery and pressure drop were monitoring throughout the whole displacement process allowing the displacement mechanisms to be inferred from the data and compared. The effect of Alberta heavy oil on the foam stability was investigated.

Chapter Two: BASIC THEORY AND LITERATURE REVIEW

In this chapter, heavy oil properties and oil recovery principles will be discussed and the field application and lab research about several non-thermal recovery methods will be presented. Besides, low field Nuclear Magnetic Resonance (NMR) and x-ray CT scan technology is also briefly introduced.

2.1 Heavy Oil Definition

Definitions of heavy oil are different depending on the author. Heavy oil is typically defined as a crude oil of less than 20 API and a viscosity above 1000 mPa.s (Dusseault, 2001). Some suggest that heavy oil should be defined in terms of producibility (Veil et al, 2009), e.g., the heavy oil should be defined to have some mobility under naturally existing condition whereby it can flow to wells and be produced. In contrast, extra heavy oil, oilsands and bitumen do not flow naturally. They are produced through thermal techniques or solvent addition.

2.2 Heavy Oil Problem

Heavy oil has very low mobility because of its high viscosity, even though its relative permeability may be close to unity. The primary and secondary recovery of such oil is not very effective. For typical 25 ° API crude oil, its primary recovery can only reach 5%-10% of total original oil in place. Water flooding promotes the recovery to about 15%. For heavy oils, such as heavy oil in western Canadian reserves, whose viscosities range from 1000 to more than 10,000 mPa.s, the mobility ratio is very unfavorable and severe viscous fingering is common during any flooding process. Hence, water flooding exhibits even poorer sweep efficiency (Miller, 2005) than conventional crude oils.

2.3 Principles of Oil Recovery

Oil recovery operations traditionally have been subdivided into three stages: primary, secondary, and tertiary. Historically, these stages described the production from a reservoir in a chronological sense.

Primary production makes use of the natural energy present in a reservoir to displace oil to producing wells. These natural energy sources include the expansion of solution gas released from the oil in the reservoir, the expansion of a gas-cap, aquifer influx, fluid and rock expansion, and gravity drainage. Secondary recovery is usually implemented after some primary production and involves the injection of water or gas to displace oil toward producing wells. Tertiary recovery (also called enhanced oil recovery) is usually implemented to displace additional residual oil after a secondary process becomes uneconomical (Lake, 1989). Examples of tertiary recovery are the injection of gas or liquid chemicals and/or the use of thermal energy. Hydrocarbon gases, CO_2, N_2, and flue gases are among the gases used in EOR processes. Tertiary recovery processes are essential for heavy oil because its high viscosity leads to low primary and secondary recovery.

Among the numerous factors influencing oil recovery, sweep efficiency and displacement efficiency are two key elements, (Green et al., 1998). Sweep efficiency is defined as the volume fraction of the reservoir contacted by the injection fluid, while displacement efficiency is the fraction of oil in place that's swept from a unit volume of the reservoir. Thus, the improvement of sweep efficiency and displacement efficiency are important for oil recovery.

There are two essential concepts for oil recovery: Capillary Number and Mobility Ratio (Ali et al, 1994). Capillary Number is defined as a dimensionless number that compares viscous forces to capillary forces as follows:

$$N = \mu v/\sigma$$ **Equation 2-1**

where,

μ= the displacing fluid viscosity, σ = interfacial tension, and v = the Darcy velocity of the fluid.

If the capillary number is large enough, the viscous force from flowing reservoir or injection fluids will overcome the capillary force which traps the residual oil in the pore. Therefore, additional oil can be displaced and the displacement efficiency will be improved. The capillary number can be increased, and the residual oil saturation decreased, by reducing oil viscosity, increasing pressure gradient, and decreasing the interfacial tension (IFT), (Taber, 1969). In most cases, a significant reduction of IFT is required to mobilize the residual oil after a waterflood.

Mobility is defined as the ratio of effective permeability to the viscosity of a given phase. The mobility ratio is the mobility of the displacing fluid divided by the mobility of the displaced fluid. At low capillary numbers, the mobility ratio determines the displacement efficiency of a displacement process. Briefly, the production rate of the displaced and displacement fluid are set by the mobility ratio which in turn depends on the saturations of the fluid in the reservoir. The saturations are determined from the material balance of injected versus produced fluids. Hence, the entire process, at least for the part of the reservoir contacted by the displacement fluid, is dictated by the mobility ratio.

The mobility ratio also affects the sweep efficiency. Ali et al (1994) pointed out the sweep efficiency decreases as the mobility ratio increases. In other words, if the displacing fluid flows more readily than oil, the displacement is inefficient on a macroscopic basic. If the mobility ratio decreases, the volume fraction of the reservoir that is contacted by injected fluids will increase, thus the sweep efficiency is increased. Sweep efficiency can be a significant factor in heavy oil reservoirs where viscous

fingering occurs. Viscous fingering is the formation of small channels through which the displacement fluid can flow without contacting addition oil.

Both increasing viscosity of the displacing fluid (e.g., by adding polymer into displacing fluid), or decreasing viscosity of the displaced oil (such as thermal technology to decrease oil viscosity), can improve the mobility ratio and therefore improve oil recovery.

2.4 EOR Process Categories

There are five broad categories in EOR processes: mobility control, chemical flooding, miscible flooding, thermal methods, and new developing technologies.

Mobility control (polymer flooding, foam flooding, etc.) is a process which is used to modify the relative rates of displacing and displaced fluid when they move through the porous media. The purpose of mobility control is to improve the displacement and volumetric sweep efficiencies; for instance, if the viscosity of injection fluid increases, its mobility decreases, the displacement process becomes more stable, and the volume fraction of oil that is swept by displacing fluid will increase. Similarly, the sweep efficiency improves when the viscosity contrast between the two fluids is reduced.

Chemical flooding (the injection of the chemical, such as surfactant flooding) mainly relies on a combination of optimum phase behavior and interfacial tension (IFT) reduction between the displacing and displaced fluid, leading to improvement of the displacement efficiency. Surfactant floods may involve microemulsions which provide ultralow IFT and high oil solubilisation (Holm, 1980). A considerable reduction of residual oil saturation is achieved during water flooding only if the IFT is reduced from 10 to 30 mN/m (in a typical waterflood) to approximately 0.001 mN/m (Green et al, 1998). In some cases, several physical or chemical interactions can lower oil viscosity thus improve microscopic displacement efficiency. Chemical flooding has been successfully applied to crude oils with high acid number and relatively low API gravity.

Miscible flooding requires miscibility between the injecting fluid and the displaced oil. In this case, the capillary number increases significantly and the microscopic displacement efficiency can be improved greatly, leading to high oil recovery (Green et al, 1998).

Thermal technologies depend on increasing the reservoir temperature and reducing heavy oil viscosity by the injection of thermal energy or the in-situ generation of heat. Reducing the viscosity of the heavy oil increases the oil mobility, leading to a decrease in the water cut and higher recovery factors. Thermal recovery processes have been applied to reservoirs with a large amount of heavy oil and oil sands that could not be produced economically with conventional oil recovery methods. In many reservoirs with extra heavy oil, primary recovery can only remove a very small percentage of original oil in place. In some extreme cases, primary recovery can be negligible. Generally, thermal recovery techniques are successful for thick pay zones with no bottom water. However, heat losses can be considerable in thin formations or those areas containing bottom water, making the application of thermal methods unattractive.

2.5 Non-Thermal Methods for Heavy Oil Recovery

Reservoir and production engineers encounter tremendous difficulties from thin heavy oil formations in Western Canada. Such formations are considered too thin for applications of thermal techniques. However, the application of non-thermal recovery methods, such as chemical recovery processes, can be economically feasible in such reservoirs. In particular, for thin heavy oil formations with oil viscosity between 100 and 2000 mPa.s, chemical flooding provides opportunities for additional recovery (Green et al, 1998). In this viscosity range, the oil is sufficiently mobile for a non-thermal displacement to be effective.

2.5.1 Waterflooding

In general, waterflooding is performed as a secondary recovery process at the end of primary production. It is widely accepted as secondary recovery technique. There are many successful waterflooding projects in heavy oil reservoirs, which show economical

incremental oil recovery. However, the reported recovery of waterflood ranges from 1% up to 20% original oil in place (OOIP) for these reservoirs (Kumar et al., 2008). Based on the observed performance of Canadian heavy oil waterflooding projects, Miller (2006) stated that the process of evaluating waterflooding performance should be empirical instead of theoretical, which means in order to understand waterflooding in heavy oil reservoirs, observation of the process in the field plays a more important role than understanding the fundamental principle involved. There are many reports about waterflooding projects in Canadian heavy oil reservoirs revealing that primary waterflooding exhibits very poor sweep efficiency due to the extreme adverse mobility ratio. Waterflooding projects exist in the Lloydminster, Saskatchewan region where the oil viscosity ranges from 500 to over 4,000 mPa.s. Very poor incremental recoveries were obtained through waterflooding and it was not an economical oil recovery method in those reservoirs (Jameson, 1973).

2.5.2 Polymer Flooding

The polymer flooding technique was introduced in the 1960s to improve the mobility ratio between the displacing water and displaced heavy oil. During the 60s-70s, polymer flooding technology was studied and field tested in many countries. Nowadays, polymer technology has been a widely applied mobility control process. In order to increase the water viscosity, water-soluble polymers with high molecular weight are diluted in the displacing water thus increasing the water viscosity significantly. Displacement and volumetric sweep efficiencies correspondently increase and thereby the efficiency of water flood improves (Green et al., 1998).

Researchers at the Daqing Oilfield made a significant breakthrough in polymer flooding technology (Wang et al, 2001) based on polymer flooding experiments in a microscopic model. They found that, in the microscopic experiment of percolating flow, both volumetric sweep efficiency and microscopic displacement efficiency can be improved by polymer flooding, not only because of its high viscosity and low mobility, but also for

its viscoelastic properties which can mobilize oil droplets trapped by capillary forces and residual oil in dead end pores.

Needham and Doe (1987) reviewed about 27 polymer flooding projects in the field. Partially hydrolyzed polyacrylamide was chosen as injection chemical in more than twenty of the projects. Of the 27 floods, 23 were essentially secondary operations, initiated at WOR less than 10. The average polymer flood recovery from those case histories is approximately 8% OOIP. The average amount of polymer injected is around 0.011 kg/m^3 of reservoir. Four of the floods were tertiary applications, initiated at WOR's of 30 to 100. Floods produced an average of 1.8% OOIP for a polymer usage of approximately 0.018 kg/m^3 of reservoir. Thus they conclude that polymer flooding has much greater potential as a secondary process than in post-waterflood applications. The averages presented above indicate roughly four times the potential recovery for a secondary compared to a tertiary flood. They speculated that there more potential for improvement while the oil was mobile and the oil permeability was relatively high.

2.5.3 Alkali-Surfactant Flooding (ASP)

Chemical flooding processes involve the injection of chemicals that decrease the IFT between the displacing phase and oil phase, improving the displacement efficiency to recover more oil.

Surfactant flooding consists of the injection of one or several surfactants, which sufficiently lower the interfacial tension between the aqueous phase and oil phase. The reduction in IFT and the resulting reduction in residual oil saturation are the expected effects. The efficiency of the surfactant in mobilizing the oil phase is affected by reservoir fluids with high salinity and hardness ions as well as surface minerals. That is one of the reasons that many tests were seen to be technologically successful but not economically feasible (Krumrine et al., 1982). Another reason is the adsorption of surfactant on the reservoir rock reducing the effective concentration of the surfactant at the water-oil interface where displacement is desired.

When alkali is added to the chemical solution, the whole system can neutralize the high content of organic acids in heavy oil and form in-situ co-surfactants. With the assistance of these in-situ surfactants, oil-in-water emulsion can be generated and produced, and this emulsion has much lower viscosity than the original heavy oil (Krumrine et al., 1982). In this way heavy oil can be entrained in the aqueous phase and produced out of the reservoir.

Krumrine et al. (1982) conducted laboratory studies to examine the effects of alkali on dilute surfactant systems which were aimed to improve oil recovery. The laboratory results showed that the combination of high pH surfactant/alkali solution, not only reduced the IFT between oil and water, but also sufficiently reduced retention of surfactant. This combination improved recoveries of residual oil from 40% to 70% with only 0.25% alkali.

ASP combination flooding is defined as a flooding system which consists of alkali, surfactant, and polymer. This chemical combination offers several advantages. The mobility ratio can be significantly improved by the injected polymer. The effective water permeability can be reduced due to the adsorption of polymer onto the reservoir rock. More residual oil can be emulsified and mobilized with the assistance of the surfactants which are generated in situ by the chemical reactions between the injected alkali and the organic acids in the crude oil. Also, the added surfactant can enhance the salinity tolerance of the alkali (Healy, 1976). In addition, the reservoir rock surface becomes more negatively charged, which not only prevent the adsorption of anionic chemicals such as anionic surfactants and polymers, but also alters the wettability of the rock surface to reduce the residual oil saturation (Miao, 1988).

ASP flooding shows satisfactory recovery feasibility for a Saskatchewan’s medium oil sample, (Zhang, 2003). The core flooding they conducted showed 23-41% oil recovery. From August 1992 to February 1994, ASP injection project (1998) was operated in China

Gudong oil field. The total injection reached 0.592 PV. As a result, oil recovery of ASP flooding in Gudong oil field increased by 13.4% OOIP, which indicated that this ASP pilot was successful. Also, data from various surveys and results of numerical simulation prove that ASP flooding improved sweep volume and increased flooding efficiency (Qu et al, 1998).

In the Daqing oilfield, many ASP flooding methods have been tested (Gao, 2010). In order to increase oil recovery and provide technical and practical experience for expanding the ASP pilot, four alkali-surfactant-polymer flooding pilot tests were conducted. From those ASP pilot tests, they concluded that ASP flooding can form an oil bank, greatly lower water cut, and increase the oil production as well as the oil recovery. The incremental oil recovery was approximately 20% over waterflooding.

2.5.4 Foam Flooding

Foam is a dispersion of gas in a liquid where the liquid phase is continuous and the gas phase is separated by lamellae (the liquid phase that separates the gas phase). In general, if bubbles of gas can be injected more rapidly than the liquid between gas bubbles drains away, a foam structure can be formed in liquid.

The foam lowers the gas mobility in the swept or higher permeability parts of the formation because the foam has a greater apparent viscosity than the displacing medium. A decrease in gas mobility diverts some displacing medium into other previously un-swept parts of the reservoir, resulting in the recovery of the additional oil (Zhang et al., 2000).

Wang et al (2001) reported the results of ASPF (Alkali-Surfactant-Polymer-Foam) flooding tests in the field, including a reservoir description, well patterns, composition of the injected ASPF, injection and production conditions and problems encountered. Field tests showed that the current recovery factor was already 65.6% OOIP. Stable foams were formed in the formation and, due to ASPF flooding, the volumetric sweep

efficiency increased and the final recovery was around 70% OOIP. However, high injection pressure at the wellhead was the major problem encountered in the field tests. It caused the lowering of the gas-liquid ratio.

Foam was injected and created in the Snorre field (Blaker et al., 2002). This treatment resulted in a gas oil ratio reduction of more than 50% over a period of 2 months, resulting in significantly increased oil production. In a heavy oil field of China, (Zhang, 2000), foam was also used as mobility control for alkali surfactant flooding. With the aid of aqueous foam, flow resistance can be controlled, thus subsequently improving heavy oil recovery. Polymer enhanced foam provides a much more stable state than conventional foams, because it has exceptional high effective viscosities (Sydansk, 1993). Foam gel has a very good effect as an agent of mobility control and profile modification (Kantzas et al, 1997 and Wassmuth et al 2000). When the oil well was producing at an excessive gas oil ratio, foam can be used as the agent to block the gas (Dalland, 1997).

In summary, core flooding tests and field tests shows that the polymer flooding, ASP flooding, and ASPF flooding can greatly enhance the oil recovery, by improving displacement efficiency and sweep efficiency.

2.6 The Application of Low Field Nuclear Magnetic Resonance

Low field nuclear magnetic resonance (NMR) is used to measure the relaxation time of protons in the sample. A static magnetic field is initially applied. The electron spins of these protons orient under this field. Then, a second oscillating field is applied which causes the change of direction of the electron spins. Because the oscillating field is constantly removed, electron spins return to their first oriented direction. The time that electrons spend to return to their oriented direction is called relaxation time. The analysis of the relaxation time of protons in a sample along with the amplitude of the signal can give a value for the porosity of the sample and fluid saturations (Coates, 1999).

2.7 X-ray CT Scan Technology

Computerized Tomography is a non-destructive imaging technique that uses X-ray technology and mathematical reconstruction algorithms to view cross-sectional slices of an object. In petroleum industry, CT scan technology is mainly used in two areas: fluid flow characterization and core description.

Several researchers used CT scanning to study variety of EOR techniques including different chemical processes. With the aid of CT scan, researchers monitor fluid movement, quantify saturation distribution and changes inside the cores during fluid flow.

2.7.1 CT Scanning Principles

When the X-ray source rotates around an object, the attenuation of the X-ray beams occur once the beams penetrate the scanned object at different angles. During the scanning process, series of detectors records the transmitted X-ray intensity data. These projections, could generate a cross sectional slice through the core by reconstruction from the computer. A three dimensional image can thus be reconstructed from the cross-sectional slices. Its working principle is shown in the picture below:

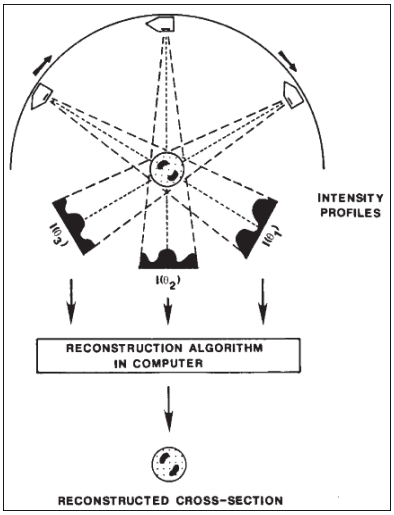

Figure 2-1: CT working principle (Willington and Vinegar, 1987)

2.7.2 CT Scanning Applications

In the last 28 years, CT has proved itself to be a reliable tool for the petroleum engineers. For special core analysis procedures and general lithologic determinations, CT is widely used to screen cores. In the research part, CT is used to study heterogeneities. Besides that, it is also used for different core flooding tests, such as miscible and immiscible EOR flooding process, relative permeability measurements, multiple-fluid flow studies and steamfloods (Willington and Vinegar, 1987).

X-ray computerized tomography was used to measure the residual saturations and porosity distributions in heterogeneous carbonate cores. Hicks *et al.* (1992) studied two different cores, and they presented the relationship between residual saturation and porosity. This work demonstrated that X-ray CT scanning is a reliable tool to experimentally measure distribution of saturation and distributions of porosity in laboratory core samples. Their work proves that X-ray CT scan can measure porosity and residual saturation distributions even in a core on a very small scale. In my study, the distribution of porosity and saturation will also be measured by the same CT technology.

Chapter Three: EXPERIMENTAL METHODS AND PROCEDURES

Chapter Three introduces the experimental preparation and displacement procedures used in the laboratory. The preparation and optimization of chemical solutions are presented, the experimental equipment is introduced and data analysis methods are discussed.

3.1 Materials and Preparation of Solutions

3.1.1 Materials

The oil samples used in the coreflood tests were collected from the Alberta Lloydminster reservoir. At atmospheric pressur e and room temperature, the density and viscosity of the cleaned dead oil was measured to be 942 kg/m^3 and 497 mPa.s. Based on NMR measurements, no emulsified water or solids were found in the oil.

Sodium chloride (NaCl) obtained from FloChem Ltd. Company was used as electrolyte in the water solution, polymer solution and ASP solution. The synthetic brine contained 0.5 wt% dissolved NaCl, and its density and viscosity were measured to be 998 kg/m^3 and 1 mPa.s, respectively, at atmospheric pressure and room temperature.

The alkali evaluated in this study was sodium carbonate which was obtained from FloChem Ltd. Company.

Nitrogen (N_2) with purity of more than 99.9% obtained from Praxair Inc. was used as the gas phase for foam generation and flooding.

3.1.2 Preparation of Chemical Solution

The polymer used in this study was Flopaam® 3630s which was provided by SNF Inc. This polymer is an anionic acrylamide copolymer with a molecular weight of 20 million Daltons.

A Corning PC-420D electrically powered magnetic stir plates were used to mix the brine and polymer solutions. The polymer powder was mixed with deionised water at low shear rate until it was completely dissolved. The final polymer solution was usually prepared by diluting a concentrated polymer stock solution. For the high molecular weight polymers used in this study, the polymer stock solution was 5,000 parts per million (ppm) of polymer in deionised water. The target polymer solution was obtained by pouring a predetermined amount of the polymer stock into a stirred solution of synthetic brine.

For instance, to prepare a 2,500 ppm polymer solution from a 5,000 ppm polymer stock solution, the following steps were followed:

1. Add 0.5 wt% NaCl to DI water to as synthetic brine.
2. Put 1,000cm^3 of the brine in a beaker and place on a magnetic stir plate then began mixing using the stirrers.
3. Slowly pour 1,000 cm^3 of the polymer stock solution (5,000 ppm polymer) into the brine.
4. Seal the beaker and allow mixing for at least 8 hours. Because these were high molecular weight polymers, 8 hours mixing might be required.

In order to hydrate the polymer, the solution was stirred for a minimum of 8 hours. Otherwise, un-dissolved polymers formed agglomerates which were surrounded by a partially dissolved jelly-like mass (called fish eyes). After the hydration time, the polymeric solutions appeared homogeneous and all fish eyes in the solution were dissolved.

The foaming surfactant used in the displacement tests was Petrostep C1 supplied by Stepan Company. Typical product properties are given in Table 3-1. Note that the actual surfactant concentration was only about 40 wt%. Both Petrostep C1 and Petrostep C2 are shown in Table 3-1, which indicates the difference of specific gravity, viscosity and percent volatile between C1 and C2. After surfactant screening tests, Petrostep C1 was chosen for the core flooding.

Table 3-1: Surfactant properties

	Petrostep C1	Petrostep C2
Water composition	58%-60% (weight percent)	54%-57% (weight percent)
Sodium (C14-16) Olefin Sulfonate	39%-41% (weight percent)	42%-45% (weight percent)
Physical state	Liquid	Liquid
Form	Liquid	Liquid
pH	8.5 at 10% Aqueous	8.5 at 10% Aqueous
Vapor density	Estimated lighter than air	Estimated lighter than air
Specific gravity	1062 kg/m^3	1063 kg/m^3
Viscosity	126mPa.s at 25℃	129mPa.s at 25℃
Percent volatile	58%-60%	59%-64%

3.2 Solution Properties Measurements

Viscosity

A Brookfield DV-III ultra programmable rheometer with cone/plate geometry was used to measure shear stress and viscosity at given shear rates. All measurements were conducted at ambient pressure and room temperature.

The principle of operation of the DV-III Ultra was to drive a spindle (which is immersed in the test fluid) through a calibrated spring. The viscous drag of the fluid against the

spindle was measured by the spring deflection. Spring deflection was measured with a rotary transducer. The viscosity measurement range of the DV-III Ultra (in centipoises) was determined by the rotational speed of the spindle, the size and shape of the spindle, the container the spindle was rotating in, and the full scale torque of the calibrated spring. The viscometer was capable of measuring viscosity to within $\pm$0.1 mPa.s. The accuracy was 0.1% based on the error between measured viscosity and true viscosity during calibration. Two measurements were conducted for each sample, and the repeatability reached $\pm$1.3 mPa.s based on 90% confidence interval.

Viscosities of both polymer solution and ASP solution were measured at room temperature (25℃) as a function of shear rates. Note the polymer solution is non-Newtonian and its viscosity was measured over a range of shear rates from 0.1 s^{-1} to 100 s^{-1}.

Density

Density was measured with an Anton Paar DMA 46 density meter. The density meter was capable of measuring densities to within $\pm 5\times10^{-4}$ g/cm^3. The accuracy was 0.03% based on the error between the known density of water and measured density of water. Two measurements were conducted for each sample, and the repeatability reached $\pm 3\times10^{-4}$ g/cm^3 based on 90% confidence interval.

Surface Tension

Foams were stable mixtures of a gas dispersed in a liquid base material. The foamer was a surfactant that facilitated the dispersion of the gas into the liquid phase by lowering the surface tension， and also stabilize the resulting foam structure (Lin et al, 2009). Surface tension of the surfactant solution was measured by a Kruss K12 tensiometer. The goal was to obtain the Critical Micelle Concentration (CMC), by using different concentration of Petrostep C1.

A container with the surfactant solution was lifted up to the lower edge of a platinum plate until the liquid entered into contact with the plate. The pulling force of the liquid at the plate was a linear measure of the surface tension of the solution. The surface tension is given by Equation 3-1:

$$\sigma = F_w / L\cos\theta \qquad \textbf{Equation 3-1}$$

where, F_w =Wilhelmy force, L=Wetted length, θ =Contact angle between liquid and platinum plate.

Note that with the use of a platinum plate it can be assumed that the contact angle was 0, and therefore $\cos\theta$ was one. For each concentration of surfactant solution, a new solution was prepared. Two measurements were taken at each concentration to ensure satisfactory repeatability, which was $\pm$0.04 mN/m based on 90% confidence interval. The accuracy reached 0.07% based on the error between measured value and true value of air-water surface tension. The precision was 0.01 mN/m.

3.3 Alkali Concentration Optimization Based on IFT Measurements

A Spinning Drop Tensiometer (Site 04-Kruss) was used to determine the interfacial tension of chemical solution (or water) against heavy oil at room temperature. In this method, a drop of the less dense fluid was injected into a container of the denser fluid, and the whole system was rotated at a preset speed. In the resulting centrifugal field, the drop was elongated along the axis of rotation. Interfacial tension opposed the elongation because of the increase in area and a configuration that minimized the system free energy was reached. The tensiometer was capable of measuring IFT within $\pm$0.01 mN/m. The accuracy reached 0.4% based on the difference between measured IFT and true IFT of known oil sample. The IFT between oil and solution (or water) can be determined using the following equation (Liu et al 2006):

$$\sigma = 3.42694 \times 10^{-7}(\rho_h - \rho_d)\omega^2 D^3 \qquad \textbf{Equation 3-2}$$

where, σ=interfacial tension (mN/m), ρ_h=the density of heavy phase (g/cm^3), ρ_d=the density of the light phase (g/cm^3), ω=the rotational velocity (rpm), D=the drop diameter (mm), and L= the length of the oil drop (mm).

The procedure for measuring interfacial tension is as follows:

1. Water (or aqueous chemical solution) was initially placed into the supply cylinder. The capillary tube was then flushed with the 150 ml aqueous solution to ensure that there were no remaining remnants of material from previous tests still in the tube. The temperature (room temperature) of the experiment was set using a water bath connected to the system.
2. A droplet of oil was introduced into the system, and the capillary tube started to rotate. The rotational speed was then increased in order to keep the oil droplet at the center of the tube and to elongate it such that its length was greater than four times its height. After the droplet reached this required length, the width of the droplet was read using the optical eye piece.
3. At the conclusion of any IFT measurement, the oil droplet would be flushed out of the tube by opening the outlet valve on the left side of the tube and allowing more chemical solution to flow into the tube that was still spinning. Finally, 500cm^3 DI water was flushed through the tube to clean off any surfactant that may have adsorbed, and to prepare the tensiometer for its next measurement.

Measurements of droplet diameter and the resulting interfacial tension were obtained as a function of alkali concentration. Note for each concentration, four IFT measurements were conducted to ensure satisfactory repeatability, which was $\pm$0.05 mN/m based on 90% confidence interval.

3.4 Foam Stability Test

The Ross-Miles method (air expansion method) was used to evaluate the stability of foams (Rojas et al, 2001). The experimental equipment used is shown in Figure 3-1. The screening tests were conducted in room temperature.

There were three parts in this test: (1) a gas cylinder, which was used to provide gas; (2) a mass flow controller that controlled gas at constant flow rate; (3) a plastic column. There was foam solution and a filter inside this column. When gas went through a porous filter, foam was generated in this transparent cylinder.

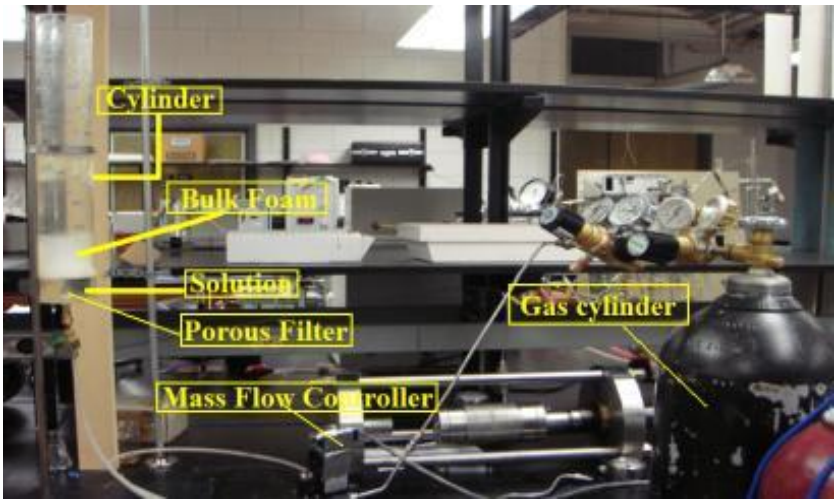

Figure 3-1: Surfactant screening tests

Bubbling was continued until 400 cm^3 foam was reached and the time to reach this volume was recorded. Then, the mass flow controller and valve were closed to stop the gas flow and the time for the foam collapsed to half its initial height was recorded. The precision was 1 s. For each concentration, two measurements were conducted to ensure the satisfactory repeatability, which was $\pm$6 s based on 90% confidence interval.

3.5 Experimental Apparatus for Displacement Tests

Figure 3-2 presented a schematic diagram of the sandpack displacement experimental set-up. If foam flooding was conducted, a mass flow controller was used to ensure the supply of the gas at a constant rate. An ISCO pump was used to inject brine and solution at a stable rate. Foam solution and gas were co-injected at fixed rates into a foam generator. They were completely mixed and formed the foam. Then foam was injected into the sandpack and displaced the residual oil. Liquid was produced and collected in the container. Differential pressure through the sandpack was monitored using the MSI absolute pressure transducers (model MSP-400). Pressure data was continually recorded and transferred into the data acquisition system. All flooding tests were conducted at ambient temperature and pressure.

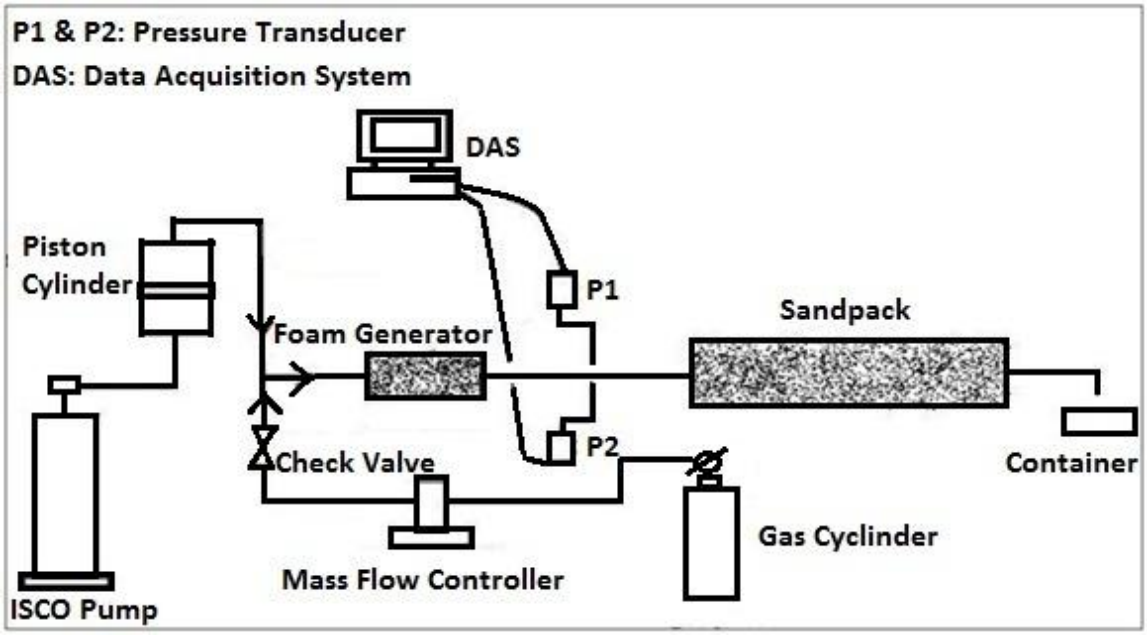

Figure 3-2: Experimental setup

Injection Pump

ISCO syringe pumps were used to inject various fluids into the porous media. This pump can be operated either in constant flow rate or constant pressure conditions. During this

work, the constant flow rate option was used for all experiments. This syringe pump had a maximum capacity of 266 cm^3.

Pressure Transducer

The function of this device was to measure and record the pressure drop across the porous media during various experiments. A series of MSI absolute pressure transducers were used during this research. The transducers were connected to a data gathering system that was installed on a personal computer. The types used for this research were 172 kPa (25 psi) and 690 kPa (100 psi) transducers.

Transfer Cylinder

This cylinder was located between the pump and the sandpack. It was used for oil flooding, water flooding, chemical flooding or foam flooding in the sandpack. Two cylinders were used, one filled with chemical (or water) for chemical (or water) flooding and the other one filled with oil for oil flooding.

Core Holder Design

The core holders were made of x-ray transparent fiber glass. Figure 3-3 indicated the structure of core holder.

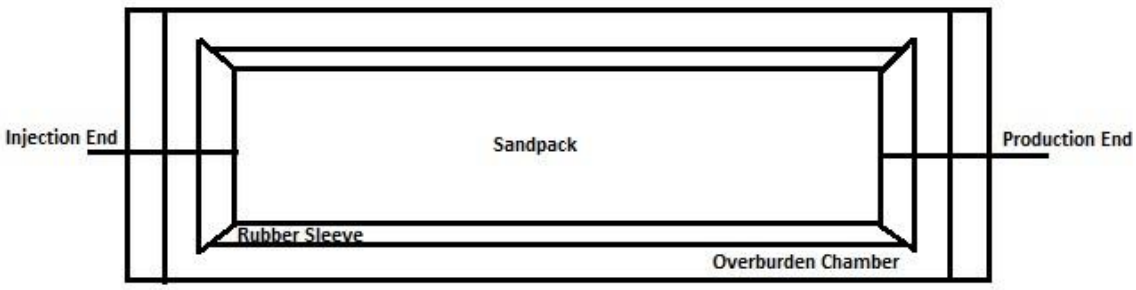

Figure 3-3: Core holder structure

The sandpack was placed inside a rubber sleeve between the core ends. In order to distribute the fluids evenly over the cross-sectional area of the sandpack, the mandrels were radially grooved. There were two mandrels, used to hold the core. In addition, a metallic fine mesh was welded on each mandrel to prevent sand from migrating out of the sandpack. Subsequently, N_2 or water was injected into the chamber. The rubber sleeve was tightened and transmitted the overburden pressure. The rubber sleeve also prevented fluids in the overburden from leaking into the sandpack. If leaking happened, the overburden material would greatly influence the properties of the sandpack. So it was very important to recognize if leaking existed. Normally, we put a transducer to record the pressure inside the core, the computer kept recording the data overnight. If the pressure data was constant, no leaking happened inside the sandpack.

Preparation of the Sandpack

Lane Mountain (LM) 50 sand was chosen as the sandpack material. Particle distribution tests were performed using sieve analysis, whereby the sand was shaken and passed through sieves with different sizes.

The particle size distribution obtained from sieve analysis ranged from 0.074 to 0.417 mm. In order to prevent fines migration through the mandrel, a mesh with 0.074 mm diameter was welded on the surface of the mandrels. All the core floods performed in this work used LM 50 sand.

The mesh to mm conversion is shown in Table 3-2. The sand was assumed to be water wet since that was the inherent nature of silica sands. The particle size distribution is shown in Figure 3-4. The average particle size was 0.292 mm with a standard deviation of 0.158 mm.

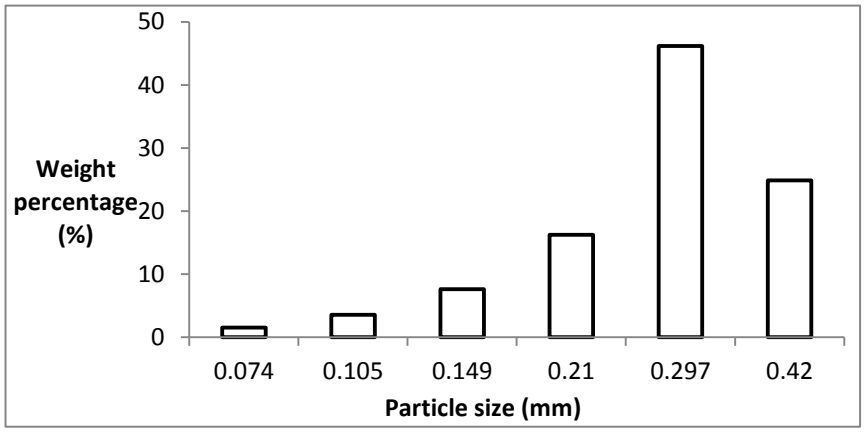

Figure 3-4: Sand particle size distribution

Table 3-2: Mesh and millimetre conversion

Mesh	mm
No. 40	0.420
No. 45	0.354
No. 50	0.297
No. 60	0.250
No. 70	0.210
No. 80	0.177
No. 100	0.149
No. 120	0.125
No. 140	0.105
No. 140	0.105
No. 170	0.088
No. 200	0.074

The sandpack was 16.0 cm long and 3.8 cm in diameter. Initially it was wet packed within a rubber tube, using methanol. The liquid level was maintained at 2 to 3 cm above the top of sand during packing process. Continual vibration was applied to ensure the packing quality. Then the sandpack was mounted inside a fibreglass core holder. An overburden pressure of 6205 kPa (900 psi) was applied to the sandpack to obtain its porosity and permeability. Then the whole coreholder was leak tested. The system was identified leak free only if there was no pressure drop with time. The sandpack was dried by injecting air for 2 days and was ready for installation into the experimental apparatus

for the displacement test. After each displacement test, it was necessary to clean the rubber sleeve and tubing thoroughly, and new sand was packed for the next test.

The rubber sleeve was secured to the mandrels (core ends) with a fine wire to prevent damage to the sandpack during handling. Then the rubber sleeve was fixed vertically on a bench, and sand was poured inside the rubber sleeve. In order to get a tighter packing, methanol was used to wet the sand. Before sand was poured in, the methanol was poured inside the rubber sleeve until the liquid level reached half height of the rubber sleeve. Then the sand was poured in, and the rubber sleeve was tapped with a plastic rod to get rid of any trapped air bubble in the sand.

After the other mandrel was put inside the rubber sleeve, the sandpack with the mandrels was carefully slid inside the core holder and secured with the end caps. An overburden pressure of 6205 kPa (900 psi) was applied using N_2 after the sandpack was completely secured and sealed. In order to confirm that there was no communication between sandpack and overburden, two valves were connected to the two ends of the core holder, one valve was closed and the other one was open and connected to a transducer with a range of 0 to 138 kPa. The pressure transducer recorded the core pressure overnight. If the pressure curve kept increasing, it means there was leaking from overburden to sandpack. Finally, the coreholder was secured vertically, and air with extremely slow injection rate flushed from the top of core holder to dry the sandpack. The whole process took 2 days to completely dry the sandpack. At this stage, it was very important to maintain the sandpack unaltered, because any change of the condition around the sandpack such as overburden pressure could modify the sandpack's properties.

The next step was flushing the sandpack with CO_2 for approximately 5 hours, followed by vacuum for another 3-4 hours. During the injection of CO_2, the core holder was secured vertically and CO_2 gas was injected from the bottom of the core to displace the remaining air out of the core. Then the core was evacuated to remove CO_2. Once vacuuming was complete, the brine was injected at constant pressure (345 kPa) to

saturate the sandpack. At the same time, the production end was closed. The pressure allowed the brine access to the pores with trapped CO_2, and dissolve CO_2. Injection continued until pressure inside the sandpack was stabilized, and no more brine was injected into the core. Then the production end was opened and the sandpack was flushed with more brine at constant rate of 30 cm^3/hr. Then CT scanning was conducted at brine saturated condition.

After the sandpack was fully saturated with the synthetic brine, it was saturated with crude oil at a flow rate of 15 cm^3/hr until there was no water production. All the displacement tests were carried out at atmospheric pressure and room temperature.

Oil at constant flow rate of 15 cm^3/hr was injected to displace the brine inside the sandpack. Vials were used to collect the produced oil and water. After the oil flooding was completed, the mass of the produced water in each vial can be determined by both NMR testing and toluene separation. Once the mass of original water inside the sandpack was known, the irreducible water saturation can be determined.

Once oil was injected into the sandpack, pressure increased steadily and a maximum pressure drop was reached at after oil breakthrough at the production end of the core. During oil flooding, pressure transducer with range of 0 to 172 kPa and pressure transducer with range of 0 to 689 kPa ranges were used to record the pressure data. The purpose of using two transducers with different range was to maintain accuracy. Pressure data were recorded initially with the lower range transducer, and once pressure exceeded 160 kPa, pressure was logged using the higher range transducer. Pressure was recorded during oil flooding until approximately 1.5 pore volume of oil was injected at a constant flow rate and the produced water cut was 0% by weight. This indicated that at the end of the oil flooding, the irreducible water saturation was reached.

Determination of Sandpack Properties

Once dry, the sandpack can be characterized. In this research, two methods were employed to measure the pore volume of sandpack: The pore volume was initially measured by the gas expansion method. Then CT scan was done to re-calculate the porosity. Brine permeability was chosen to measure permeability of the sandpack.

Measurement of Pore Volume and Porosity

The gas expansion method is based on the Boyle's law:

$$p_1 v_1 = p_2 v_2 \qquad \textbf{Equation 3-3}$$

The sandpack was connected to a helium gas cylinder and air inside the core was displaced by helium gas until the sandpack was fully saturated by helium. Then the sandpack was pressurized within 69 kPa (10 psig) by injecting helium gas, and the whole system was isolated. Then the sandpack was connected to degassed water cylinder by opening the appropriate valve. So the exiting gas displaced the water in the cylinder and sandpack was depressurized until the ambient pressure was reached. Thus the pore volume of the sandpack can be calculated by measuring the volume of the displaced water. Note the dead volume was also measured by gas expansion technique. Since the pressure was very low, the ideal gas law can be used for the calculations. Solving Equation 3-3 using the ideal gas relation gives:

$$V = \frac{p_1 \frac{m_1}{\rho_w}}{p_2} - V' \qquad \textbf{Equation 3-4}$$

In which, V=Pore volume, p_1-Atmosphere pressure, m_1-Mass of the water, p_2-Gauge pressure, ρ_w-Water density V'-Dead volume.

Measurement of Brine Permeability

Permeability is defined as the conductivity of the porous media with respect to permeation by a Newtonian Fluid (Dullien, 1992). Darcy's law has been widely accepted to describe the fluid transport ability in porous media. This empirical equation relates the flow rate of a fluid flowing through a porous media to the viscosity of the fluid and the differential pressure across the sample.

For linear and steady state flow of incompressible fluids, Darcy's law is defined as:

$$Q = \left(\frac{kA}{\mu}\right)\left(\frac{\Delta P}{L}\right) \qquad \textbf{Equation 3-5}$$

In this test, both helium gas and brine were used to measure absolute permeability of sandpack. However, in unconsolidated sandpacks with high permeability, low gas pressure was hard to control and measuring high gas flow rate was inaccurate. For this reason only brine permeability was used as permeability of the sandpack.

First, the brine saturated sandpack was set at a certain height. Brine was flowed through the sandpack due to hydrostatic drive, and the flow rate was recorded. The calculated pressure drop was plotted against measured flow rates. Note that the flow rate was very low, which was laminar flow, thus Darcy's law can be applied. The permeability value can be obtained from the slope of this line by using Darcy's law.

$$Q/A = k\left(\frac{dp}{\mu l}\right) \qquad \textbf{Equation 3-6}$$

where, Q=Volumetric flow rate (cm^3/s), L=Length (cm), A=Cross sectional area of the porous media (cm^2), k=Permeability (D), ΔP=Pressure drop (atm), μ =Fluid viscosity (mPa.s).

3.2 Procedure for Displacement Tests

In general, for each sandpack, the fluid was injected in the following sequence:

1. Oil flooding: Oil injection was carried out at the injection rate of 15cm ^{3}/hr until water cut was 0. Initial oil saturation was calculated after oil flooding.
2. Water flooding: The oil was displaced by injecting brine. Water flooding was continued until no oil production was observed, which means 100% water cut was found in the producing liquid. Residual oil saturation and recovery of water flooding were calculated by the mass balance method.
3. Foam or chemical injection: After water flooding, foam or chemical solution was injected until 100% water cut in the effluent was achieved.

3.3 Calculation of the End Point Mobility

Because there was one phase flow at the end of each displacement, we can calculate end point mobility based on Darcy's law:

$$\frac{k}{\mu}\frac{\Delta p}{l} = \frac{Q}{A} \qquad \textbf{Equation 3-7}$$

Oil mobility at the end of oil flooding:

$$M_o = \frac{k_{oiw}}{\mu_o} = \frac{Ql}{A\Delta p_o} \qquad \textbf{Equation 3-8}$$

where, k_{oiw}-Oil permeability at the end of oil flooding, μ_o-Oil viscosity, Δp_o-Pressure drop at the end of oil flooding.

Water mobility at the end of water flooding:

$$M_w = \frac{k_{wor}}{\mu_w} = \frac{Ql}{A\Delta p_w} \qquad \textbf{Equation 3-9}$$

where, k_{wor}-Water permeability at the end of water flooding, μ_w-Water viscosity, Δp_w-Pressure drop at the end of water flooding.

Polymer solution mobility at the end of polymer flooding:

$$M_p = \frac{k_{por}}{\mu_p} = \frac{Ql}{A\Delta p_p} \qquad \textbf{Equation 3-10}$$

where, k_{por}-Polymer permeability at the end of polymer flooding, μ_p-Effective polymer viscosity, Δp_p-Pressure drop at the end of polymer flooding.

3.4 NMR testing

In order to measure the mass of produced oil and water, NMR readings were made in an Ecotek-FT spectrometer. The data were analyzed using ExpFit software. And excel file was output. It mainly included relaxation time of hydrogen protons and the amplitude of the sample.

Morriss et al. (1997) has shown that the relaxation time was inversely proportional to the viscosity. The relaxation time for water takes about 1,000 to 3,000 ms, while the relaxation time for viscous oil is only around 10 ms. The Figure 3-5 shows the oil water signal in the produced mixture.

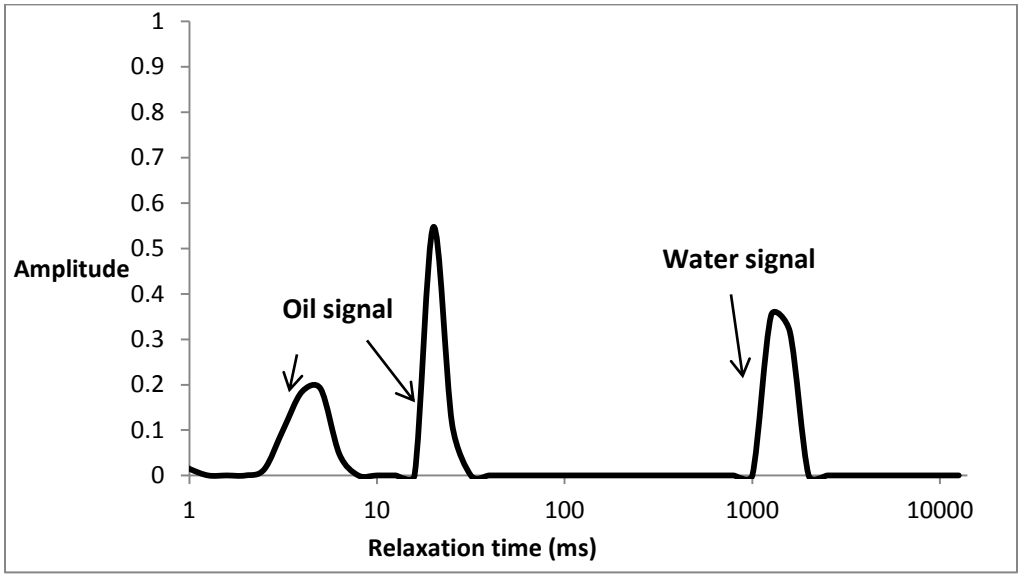

Figure 3-5: NMR singal

Because water signal is very characteristic (relaxation time ranges from 1,000 to 3,000 ms), thus within this range, all the amplitude for water signal can be accumulated. Coates et al (1999) proved that the amplitude of the signal was directly proportional to the mass of sample. So water mass can be related to the amplitude of the water signal. Mass of water can be calculated as it shows in Equation 3-11:

$$m_w = \frac{A_w}{AI_w} \qquad \textbf{Equation 3-11}$$

In which, m_w-Mass of water, A_w- Amplitudes of water signal, AI_w- Water amplitude index.

The amplitude index for water can be obtained from the relationship curve between known mass of water and its corresponding amplitude. The slope of this curve was equal to the amplitude index. After water mass was calculated by amplitude index, the oil mass can be obtained by mass balance.

In order to determine the accuracy of NMR, several water samples with known mass was

NMR scanned. As it shows in Figure 3-6, the amplitude index was equal to 0.113. Then the mass of water was calculated by amplitude and amplitude index. The error between calculated value and true value was obtained. Thus the accuracy of NMR was calculated to be 2.44%.

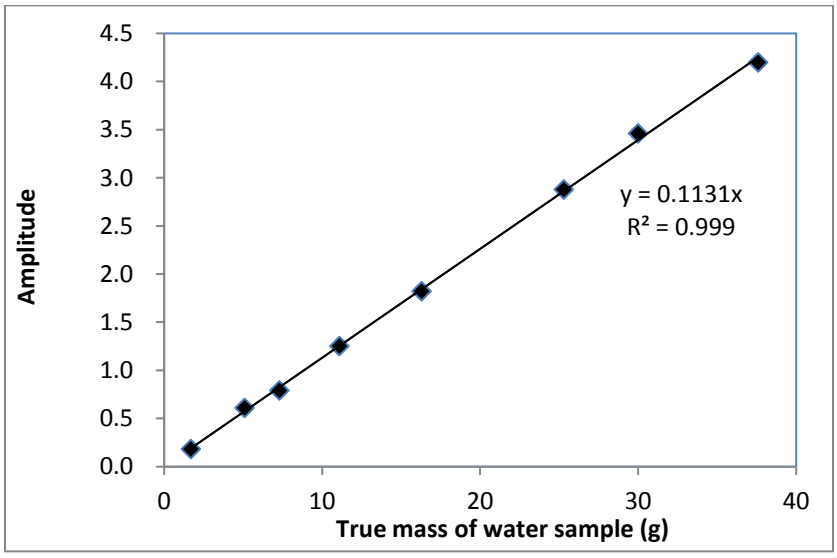

Figure 3-6: Amplitude index for water

3.5 Toluene Separation

In order to validate the accuracy of NMR testing results, toluene separation method was also used. The water oil mixture was poured in plastic funnels. Toluene was then added to the mixture, so oil and toluene became one phase, and water was the other phase. To obtain a good separation of the oil phase, a large amount of toluene was added and agitation of the funnel was required because part of the oil was emulsified in the water phase. Due to the difference in densities, the oil phase would sit at the top of the mixture. Thus water can be collected by opening the valve on the bottom of the funnel.

In order to determine the accuracy of toluene separation method, the oil and brine samples with known mass were mixed and then separated with toluene. Then the water mass was measured and compared with its known mass, as it shows in Figure 3-7. The

accuracy of toluene separation method was calculated to be 0.23%.

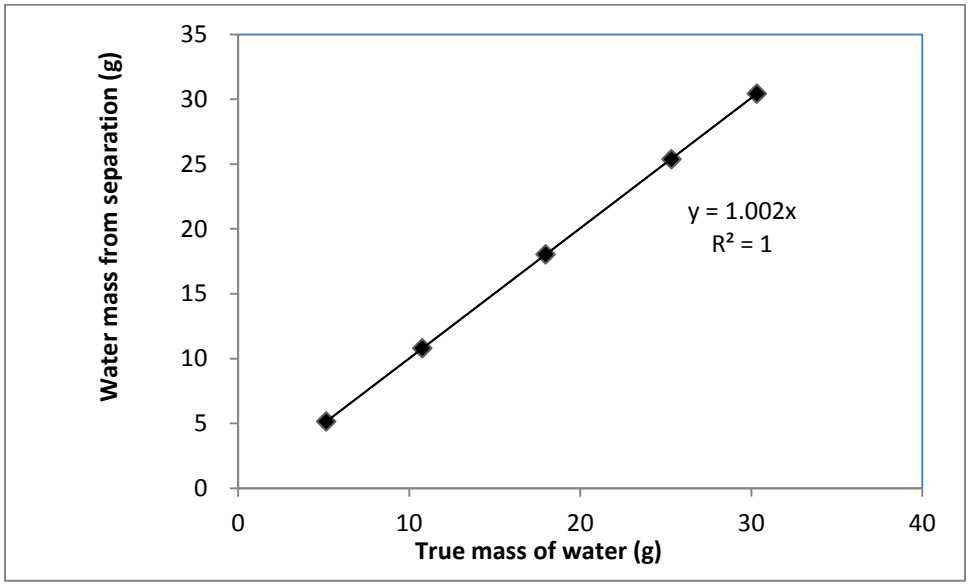

Figure 3-7: Comparison between toluene seperation and true mass

3.6 CT Data Analysis

To obtain the statistics and visual data from the sandpack samples, the major processing stages for image slices within a core sample are:

1. Transfer the CT scan raw data from the scanner into a readable format (typically a text file).
2. Separate and highlighted the sandpack ROIs (regions of interest) of the scans from the whole CT scan area.
3. Produce CT number text image files, and statistics of the scan ROIs.
4. Convert the CT number text image files and statistics of the scan ROIs to density.
5. Convert the density text image files, and statistics of the scan ROIs to porosity.
6. If necessary, convert the density and porosity text image files, and statistics of the scan ROIs to information on gas saturation.

Linear Attenuation Coefficient

The linear attenuation coefficient of x-rays passing through material of fixed density was the parameter measured in CT. It was defined from Beer's law (Vinegar and Wellington, 1987):

$$\frac{I}{I_o} = e^{-\alpha x} \qquad \textbf{Equation 3-12}$$

where, α= Linear attenuation coefficient, I_o= Incident X-ray intensity, I=Measured intensity after penetrating sample, x=Sample thickness.

Conversion of the CT Numbers to Density

CT numbers were the original output of the CT machine. A CT number can be effectively expressed as a normalized value of the calculated x-ray absorption coefficient of a location (Al-Muntasheri et al, 2010).

In this step, CT numbers could be converted to densities of scanned material by using a calibration equation. Regarding the construction of the calibration equation, at least four materials were needed. All of them were CT scanned. So the average CT numbers can be measured. By plotting measured CT number against known densities of material, a calibration equation can be created. Normally, this relationship between density and CT number was expressed as: Density = (A$\times$CT number) + B. However, the calibration equation should be updated for each CT scan. The reasons and procedures were mentioned below.

From the CT scan, the raw CT number can be obtained. However, conditions such as room temperature, humidity, atmospheric pressure had an effect on the CT number results, which made CT number drift when condition changed, which means if the same material was CT scanned in different times, the CT numbers were not the same. Only if

CT numbers were corrected, I can accurately use it to get the true calibration equation. The method was mentioned below.

The Figure 3-8 described how I generated calibration equation for the CT scan. Normally we put at least four standards into the core holder to simulate the sandpack. The whole system was under CT scan. Then I constructed calibration equation by plotting the CT numbers found for different standards against their known densities. This resulted in an equation of the form: Density = (A × CT number) + B.

However, the CT number for certain material may vary from different times of CT scan. In order to get rid of CT number drift, I put extra standard outside the core holder during CT scan, as Figure 3-8 shows. By comparing CT numbers of this standard every time I performed CT scan, I could calculate the drift of CT numbers, and this CT numbers drift caused the drift of calibration equation.

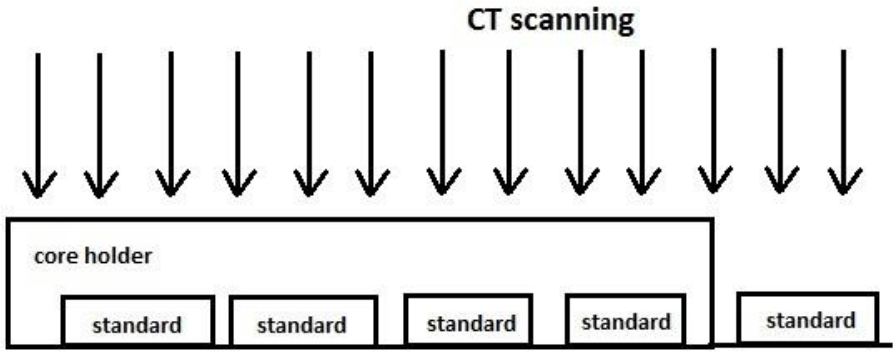

Figure 3-8: CT scanning for constructing the calibration equation

Figure 3-9 indicated the drift of calibration equation.

Line L' stood for relationship curve between CT number and density, the four points on the line stood for the four standards I used. Because their density was known, so line L' can be constructed. Point A' stood for the standard outside the core holder, because

standard outside was not in the same condition with those four standards inside, so Point A’ was not on the line L’.

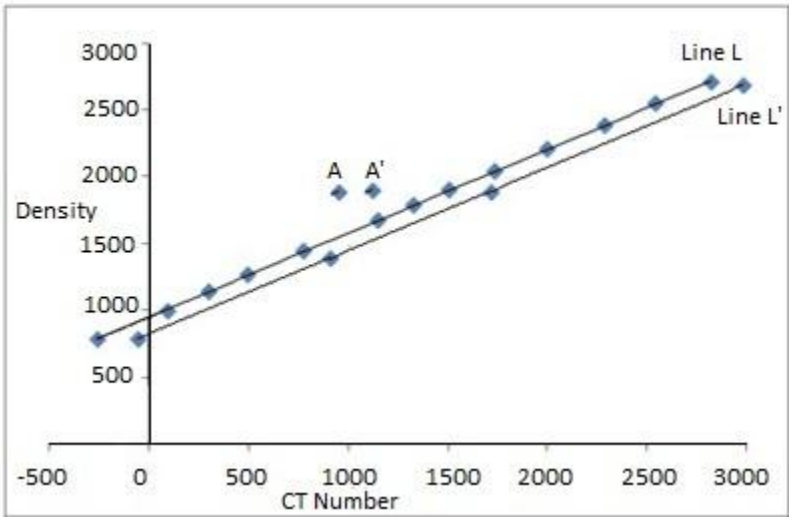

Figure 3-9: CT scanning for generating the true calibration curve

When the sandpack was put in the core holder, it was sandpack instead of four standards under the CT scan. Line L’ cannot stand for the true calibration curve of the sandpack. When I scanned the sandpack, I still kept the same standard outside the core holder, point A stood for that standard. Note that point A and A’ stood for the same standard, the density should be the same. Also note that the point A and A’ derived from different times of CT scan, thus CT number drift happened. The difference of CT number between point A and A’ was this drift. Similarly, the same CT number drift happened inside the core holder. All the points in Line L’ moved the same distance and finally formed Line L. So Line L and L’ are parallel. And line L was the true calibration curve for the sandpack.

Conversion of Density to Porosity

Porosity was the ratio of the pore volume to the bulk volume of the whole core, which could be calculated using Equation 3-13:

$$\emptyset = \frac{(\rho_g - \rho_m)}{(\rho_g - \rho_f)}$$ **Equation 3-13**

where, $\emptyset$–Porosity, ρ_g–Grain density, ρ_m–Measured density, ρ_f–Fluid density.

Grain density was the density of the pure rock, which was assumed to be 2650kg/m^3, and fluid density was the density of the fluid which resided in pore spaces. Note that the porosity was determined when there was only one phase, which could be water or air.

Gas Saturation

Gas saturation was effectively the gas volume fraction in the porosity of a core. In our work, if the porosity was known, then taking the measured density and applying equation above results in the gas saturation.

First the fluid density within the porosity was calculated as it shows in Equation 3-14. Note that the fluid mentioned was the integration of gas and liquid.

$$\rho_f = \frac{(\rho_m - (1-\emptyset) \times \rho_g)}{\emptyset}$$ **Equation 3-14**

where, $\emptyset$-Porosity, ρ_g-Grain density, ρ_m-Measured density, ρ_f-Fluid density.

From the known liquid and gas densities, the gas saturation can then be estimated:

$$f_g = \frac{\rho_w - \rho_f}{\rho_w - \rho_g}$$ **Equation 3-15**

where, f_g-Gas saturation, ρ_w-Water density, ρ_f-Fluid density, ρ_g-Grain density.

Chapter Four: EXPERIMENTAL RESULTS

In this chapter, the optimization of the alkali concentration is discussed, surfactant screening tests are presented, and the chemical properties of the displacement fluids are reported. Then, the waterflooding, polymer flooding, ASP flooding and ASPF flooding displacements are investigated and evaluated.

4.1 Optimum Alkali Concentration Determination

A series of alkali solutions were prepared using the synthetic brine, with different alkali concentrations (0, 0.1, 0.2, 0.3, 0.4, 0.5, 0.6, 0.7, 0.8, 0.9, 1.0 weight percent). To determine the optimum concentration of alkali, the minimum IFT between alkali (Na_2CO_3) solution and heavy oil phases was determined, as shows in Figure 4-1. The IFT was relatively constant above an alkali concentration of 0.5 wt%. Thus 0.5 wt% Na_2CO_3 was used as the alkali concentration. At this point, a two orders of magnitude IFT reduction was achieved. Note that after adding the 4,000 ppm surfactant (Petrostep C1) to the solution, the IFT further decreased to 0.002 mN/m.

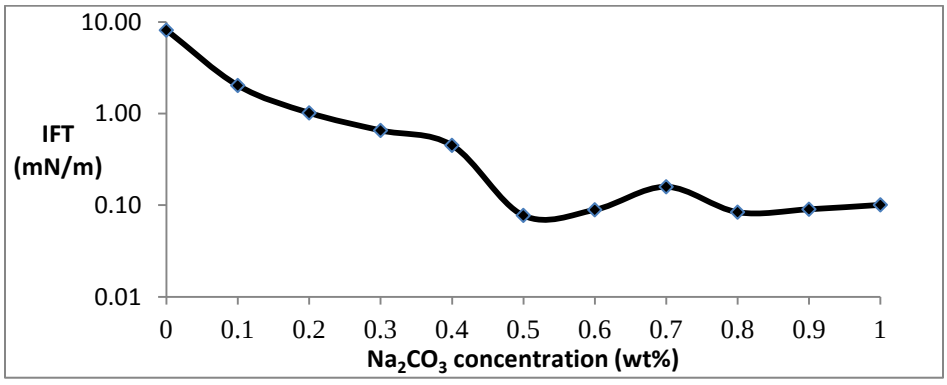

Figure 4-1: Interfacial tensions after 10 minutes between the aqueous alkaline phase and heavy oil as a function of alkali concentration (with repeatability of ±0.05 mN/m based on a 90% confidence interval).

4.2 Surfactant Screening Test

The Ross-Miles method (air expansion method) was also used to screen the surfactants Petrostep C1 and C2, Table 4-1. The foaming ability (half life) of Petrostep C1 was slightly greater than Petrostep C2. For both surfactants, the half-life increased with increasing surfactant concentration up to 4000 ppm and remained constant at higher concentrations. This effect was due to the formation of molecular aggregates micelles since it appeared near the critical micelle concentration (CMC) of 4000 ppm (see appendix for details on the cmc determination). Above the CMC, the surface tension becomes constant and the foam properties are not expected to change with increasing surfactant concentration (Rojas et al, 2001). Therefore, 4000ppm of Petrostep C1 was used as the foam solution. Note that the product Petrostep C1 was an aqueous solution of sodium olefin sulfonate. It only contained 40 wt% surfactant, which means the actual concentration of the surfactant was 1600 ppm.

Table 4-1: Surfactant screening test

Surfactant concentration	Surfactant	Foam volume that need to be generated	Gas flow rate	Rising time	Half-life time
4500ppm	Petrostep C-1	400cm^3	10cm^3/min	25min 29s	2 hr 59 min
4000ppm	Petrostep C-1	400cm^3	10cm^3/min	25min 27s	3 hr 03 min
3500ppm	Petrostep C-1	400cm^3	10cm^3/min	25 min 58s	2 hr 37 min
3000ppm	Petrostep C-1	400cm^3	10cm^3/min	26 min 19s	2 hr 04min
4500ppm	Petrostep C-2	400cm^3	10cm^3/min	27min 20s	2 hr 25 min
4000ppm	Petrostep C-2	400cm^3	10cm^3/min	27min 23s	2 hr 50 min
3500ppm	Petrostep C-2	400cm^3	10cm^3/min	27 min 44s	2 hr 15 min
3000ppm	Petrostep C-2	400cm^3	10cm^3/min	27 min 57s	1 hr 42 min

4.3 Solution Viscosity Measurement

After the concentration of surfactant and alkali was determined, 2,500 ppm was used as the concentration of polymer. Then the rheology behavior of polymer solution and ASP solution was studied. Figure 4-2 shows the viscosity as a function of shear rate for evaluated solution at room temperature.

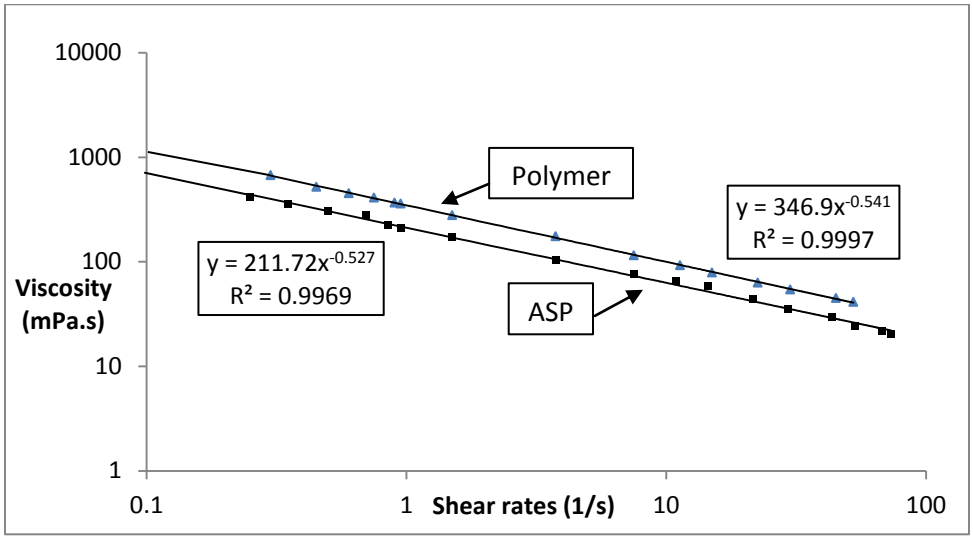

Figure 4-2: Viscosity measurements of the polymer and ASP solution

Figure 4-2 shows that the viscosity of both polymer solution and ASP solution decreased as a function of shear rate, which was typical of shear-thinning fluids. This behavior was caused by the uncoiling of the polymer chains as they were elongated in shear flow. As the shear rate increased, the polymer molecules began to untangle and align in the shear field, reducing the resistance to slippage (Rosen, 1982). In addition, the addition of alkali and surfactant decreased the viscosity of the polymer solution, which had a negative effect on the mobility improvement.

For a linear displacement, Lake's equation (Lake, 1989) can be used to measure shear rates:

$$\dot{\gamma}_{eq} = 4v\left(\frac{\emptyset}{8k}\right)^{1/2} = \frac{4q}{A\sqrt{8k\phi}} \qquad \textbf{Equation 4-1}$$

where: $\dot{\gamma}_{eq}$-Shear rate, q- Volumetric flow rate, A- Cross sectional area, k- Permeability, $\emptyset$- Porosity.

The injection rates during polymer flooding and ASP flooding were 6 cm^3/hr and 15 cm^3/hr, thus shear rates were calculated to be 1.50 s^{-1} and 3.75 s^{-1}. For polymer injection, measured dynamic viscosities under these two shear rates were 278.9 mPa.s and 175.3 mPa.s respectively. And for ASP injection, the dynamic viscosities were 172.7 mPa.s and 103.7 mPa.s, respectively. Note the viscometer was capable of measuring viscosity to within $\pm$0.1 mPa.s.

4.4 Saturating the Sandpack with Oil

Table 4-2 summarizes the oil saturations for the sandpacks. Note that for the Sandpack# 6, there was no oil flooding. The average initial oil saturation for Sandpack#2 to Sandpack#6 was 75.1%. Although oil was much viscous than water, the oil cannot displace all water in the sandpack, this was because of the capillary force. Thus, the initial oil saturation cannot reach 100%. However, the initial oil saturation for each sandpack was similar, which means the initial condition for each pre water flooding was the same.

Table 4-2: Summary of oil volume and initial oil saturation

Sandpack #	Initial oil saturation (%)
1	75.4
2	75.2
3	73.9
4	75.2
5	76.0
6	N/A

The sandpack were designed to evaluate displacement performance of the ASPF or chemical in porous media. In total, six sandpack tests were conducted. The properties of the sandpacks after the water flooding are shown in Table 4-3. The porosity, permeability and residual oil saturation were similar for each post waterflooding sandpack, thus the parameters (such as recovery efficiency, oil water ratio) for different tertiary oil recovery can be compared.

Table 4-3: Summary of sandpack properties

	Sandpack 1 (P15)	Sandpack 2 (P6)	Sandpack 3 (ASP15)	Sandpack 4 (ASP6)	Sandpack 5 foam, oil	Sandpack 6 foam, no oil
Brine permeability (Darcy)	5.69	6.01	6.01	6.03	5.55	5.69
Porosity (%)	37.0	36.9	35.4	36.2	36.9	36.3
OOIP (cm^3)	49.57	49.17	48.33	48.33	53.75	-
S_{wi} (%)	24.6	24.8	26.1	24.8	24.0	-
RF of water flooding (%)	29.8	30.3	27.1	25.8	30.7	-
μ_o (mPa.s)	497	497	497	497	497	497
ρ_o (g/cm^3)	0.9418	0.9418	0.9418	0.9418	0.9418	0.9418

After oil flooding and water flooding, the polymer, ASP or foam was injected at constant rates until the oil production was close to zero. Note that all the flooding tests were carried out at ambient conditions. All the water flooding was conducted at a constant rate of 15 cm^3/hr. For the foam flooding, 15 cm^3/hr and 80% foam quality indicated that the injection rate of foam solution was 3 cm^3/hr and nitrogen injection was 12 cm^3/hr. Also note that the repeatability of oil recovery of water flooding reached $\pm$2.0% based on 90% confidence interval, and we assume this repeatability can also be applied to the other displacement tests.

4.5 Displacement Tests Results

In order to evaluate the recovery performance of polymer flooding, ASP flooding and ASPF flooding, several sandpack displacement tests were conducted. The heavy oil with viscosity of 497 mPa.s was chosen as the oil sample. A total six sandpack tests were conducted and the sequence of displacements are shown in Table 4-4. The first two displacements were conducted as water flooding + polymer flooding at 15 cm^3/hr or 6 cm^3/hr. The polymer flooding will be compared with water flooding to investigate oil recovery mechanism of polymer flooding. Then Displacement# 1 and #2 were compared with next two displacements-water flooding + ASP flooding at 15 cm^3/hr or 6 cm^3/hr, to investigate if the alkali and surfactant contribute to extra oil recovery. Displacement #5 was conducted as water flooding + ASPF flooding at 15 cm^3/hr. It is compared with Displacement #3 to investigate if the gas contributed to the oil recovery. Displacement #6 is ASPF flooding in oil free condition. It was compared with Displacement #5 to investigate the effect of heavy oil on the foam.

Table 4-4: Summary of displacement procedure

Sandpack Test	Displacement Procedures
1	Water flooding (15 cm ³/hr)+polymer flooding (15 cm ³/hr)
2	Water flooding (15 cm ³/hr)+polymer flooding (6 cm ³/hr)
3	Water flooding (15 cm ³/hr)+ASP flooding (15 cm ³/hr)
4	Water flooding (15 cm ³/hr)+ASP flooding (6 cm ³/hr)
5	Water flooding (15 cm ³/hr)+ASPF flooding (15 cm ³/hr)
6	ASPF flooding (15 cm ³/hr) in brine saturated core

4.5.1 Water Flood at 15 cm ³/hr and Polymer Flood at 15 cm ³/hr

Displacements# 1 and #2 focused on the effect of polymer flooding on a post-waterflooding core. The initial properties of the Sandpack# 1 after oil flooding are given in Table 4-5.

Table 4-5: Initial condition of Sandpack# 1 after oil flooding

Porosity (%)	37.0
Permeability (D)	5.69
OOIP (cm^3)	49.57
Oil saturation (%)	75.4
Irreducible water saturation (%)	24.6
Oil viscosity (mPa.s)	497
Oil density (g/cm^3)	0.9418

After the sandpack was saturated with the heavy oil, the waterflood was performed at a constant flow rate of 15 cm^3/hr. 7.9 PV of brine were injected until the water cut was nearly 100% and the oil recovery was 29.8%. The oil recovery, water cut, and pressure drop as a function of injected PV are shown in Figure 4-3:

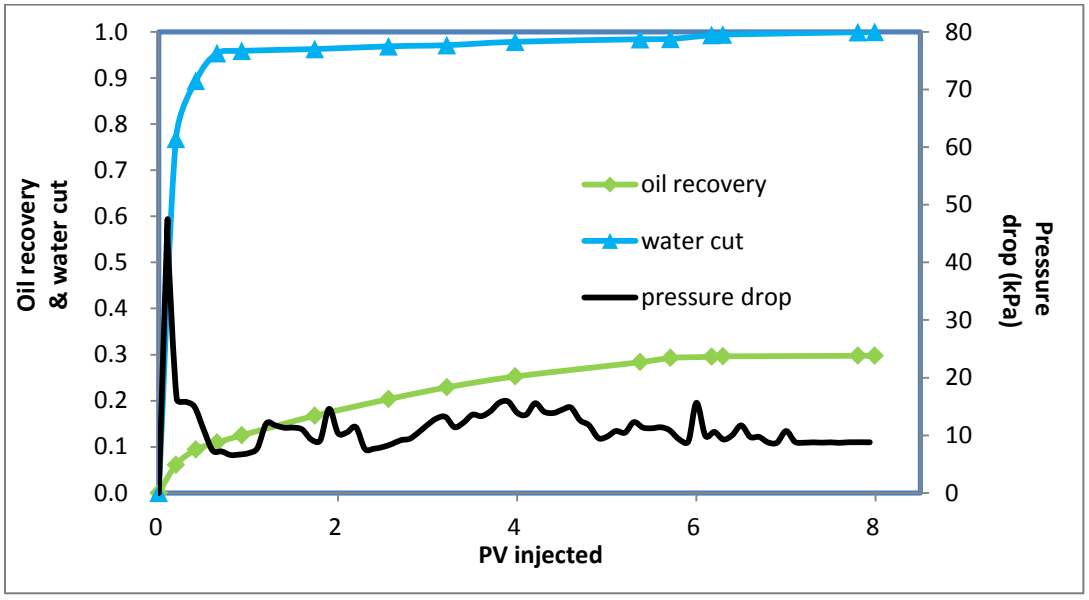

Figure 4-3: Oil recovery, water cut and pressure drop as a function of injected PV during water flooding

During waterflooding, several forces may be present (Mai and Kantzas, 2008). Before water breakthrough, the viscous force was important because water was injected into a continuous oil phase. Most of the oil was displaced as an bank at this stage. However,

because the injection rate was high, the displacement of water was unstable and water breakthrough occurred early in the life of waterflood. After water breakthough, the water flowed in water saturated channels within the largely oil saturated reservoir and therefore the pressure drop significantly decreased. An additional 20% of oil was eventually recovered after water breakthrough as the displacement progressed and the sweep efficiency improved. At the end of a core displacement, the sweep efficiency approaches 100% and therefore the ultimate recovery is dictated by the displacement efficient which in this case gives a recovery factor of 30%.

After the waterflood, the polymer was injected at a rate of 15 cm^3/hr until the oil production was close to zero. Figures 4-4 and 4-5 respectively show the oil recovery, water cut and pressure drop during polymer flooding at 15 cm^3/hr and during water and polymer flooding combined. Oil production increased until 1.3 PV of polymer was injected, with an incremental oil recovery of 49.1% OOIP (for a total oil recovery of 78.9%). The recovery summary of both water flooding and polymer flooding is presented in Figure 4-5.

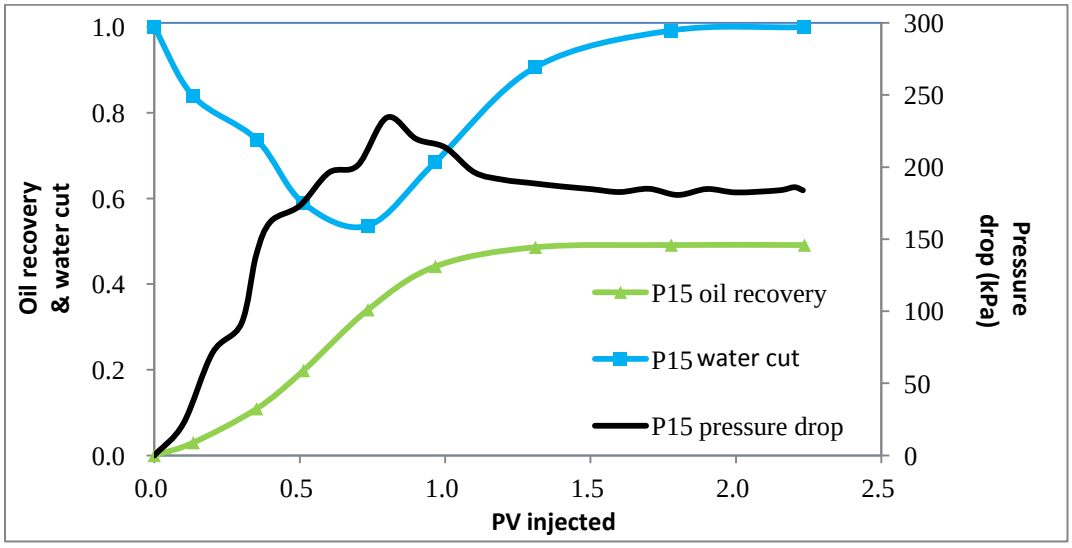

Figure 4-4: Oil recovery, pressure drop and water cut as a function of injected PV during polymer flooding at 15 cm^3/hr

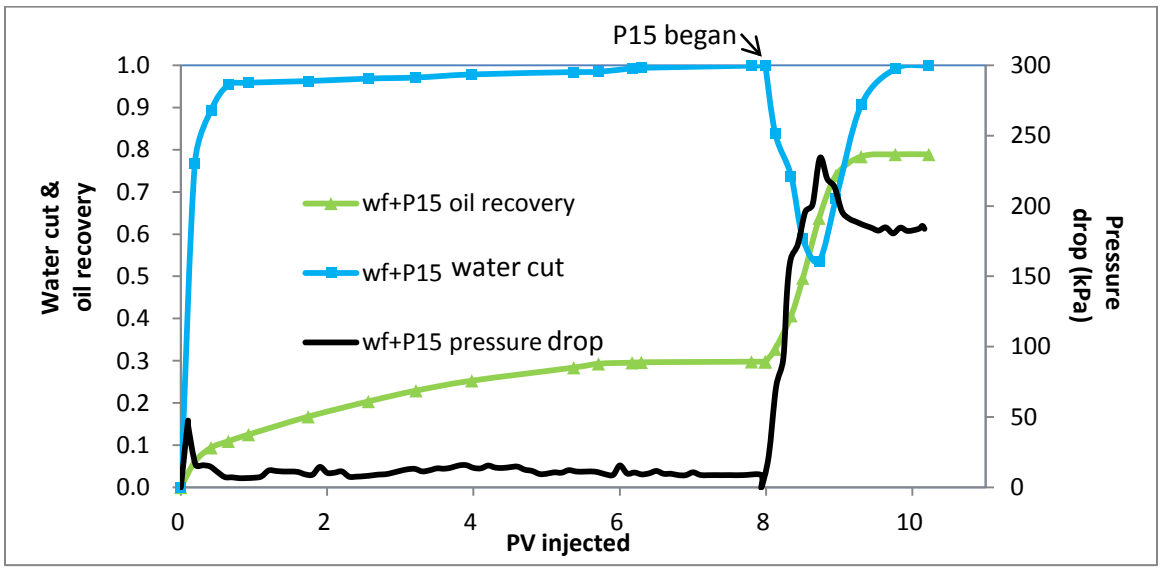

Figure 4-5: Summary of oil recovery, pressure drop and water cut for Displacement #1

The polymer flood achieves higher oil recovery because the higher viscosity of the polymer reduces the mobility ratio. A lower mobility ratio improves both the displacement and the sweep efficiency. The improved sweep efficiency gives higher recovers at a given PV injected and the improved displacement efficiency gives a higher ultimate recovery. In this case, the viscosity ratio between the polymer and the oil is 0.35:1 compared with 0.002:1 for water and oil. Hence, the viscosity ratio is reduced by a factor of 175. The end point mobility at the end of polymer flooding was 0.003, comparing with a water flooding end point mobility of 0.076.

4.5.2 Water Flood at 15cm ³/hr and Polymer Flood at 6cm ³/hr

In order to study the effect of injection rate on the heavy oil recovery, Sandpack# 2 was prepared, water flooded at 15 cm^3/hr, and then polymer flooded with an injection rate of 6 cm ³/hr. The viscosity ratio between the polymer and the oil was approximately 0.56 similar to the ratio of 0.35 for Displacement# 1. Table 4-6 presents the initial condition of the Sandpack# 2 after oil flooding.

Table 4-6: Initial condition of Sandpack# 2 after oil flooding

Porosity (%)	36.9
Permeability (Darcy)	6.01
OOIP (cm^3)	49.17
Initial oil saturation (%)	75.2
Irreducible water saturation (%)	24.8
Oil viscosity (mPa.s)	497
Oil density (g/cm^3)	0.9418

Figure 4-6 shows that the waterflood performance was similar to that of Sandpack #1. Water broke through after 0.1 PV of water was injected and the oil recovery reached 7.0% of OOIP. After water breakthrough, the pressure declined drastically and stabilized at 5 to 7 kPa. After about 7.3 PV of brine injection, the water cut approached 100%. The total oil recovery reached 30.3% of OOIP.

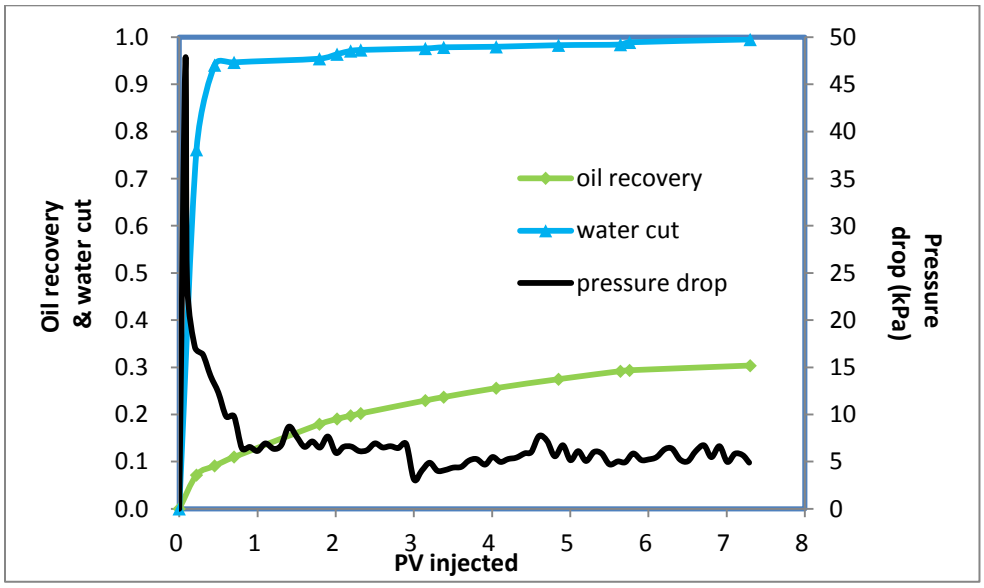

Figure 4-6: Oil recovery, water cut and pressure drop as a function of injected PV during water flooding of Sandpack #2.

After waterflooding, 2.3 PV of polymer was injected at 6 cm^3/hr until the oil production was close to zero. Figure 4-7 shows the oil recovery, water cut and pressure drop as a function of injected PV during the polymer flooding. Figure 4-8 shows the combination

of water cut, oil recovery and pressure drop during water flooding and polymer flooding. An additional 46.9% OOIP was recovered after injecting 2.3 PV of the polymer for a total oil recovery of 77.2% of OOIP. The residual oil saturation was 15%.

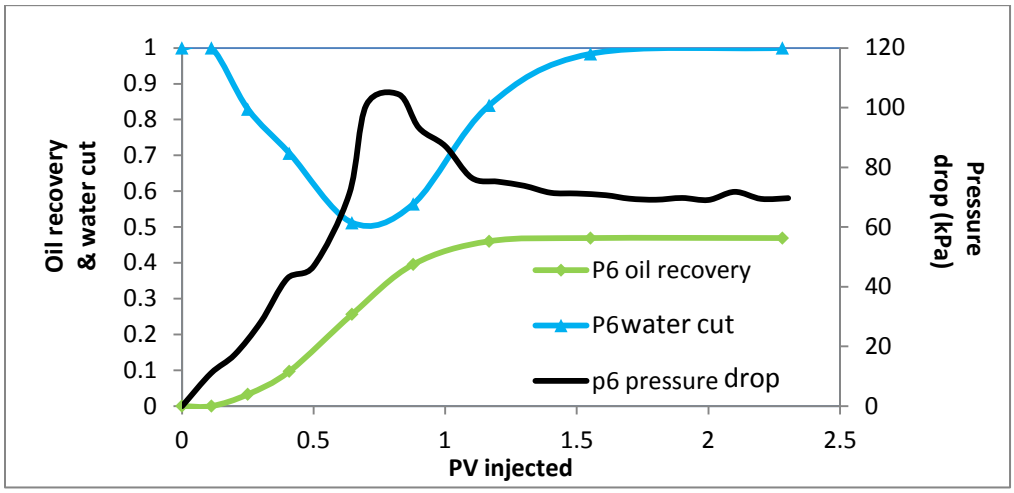

Figure 4-7: Water cut, oil recovery and pressure drop during polymer flooding of Sandpack #2 at 6 cm³/hr.

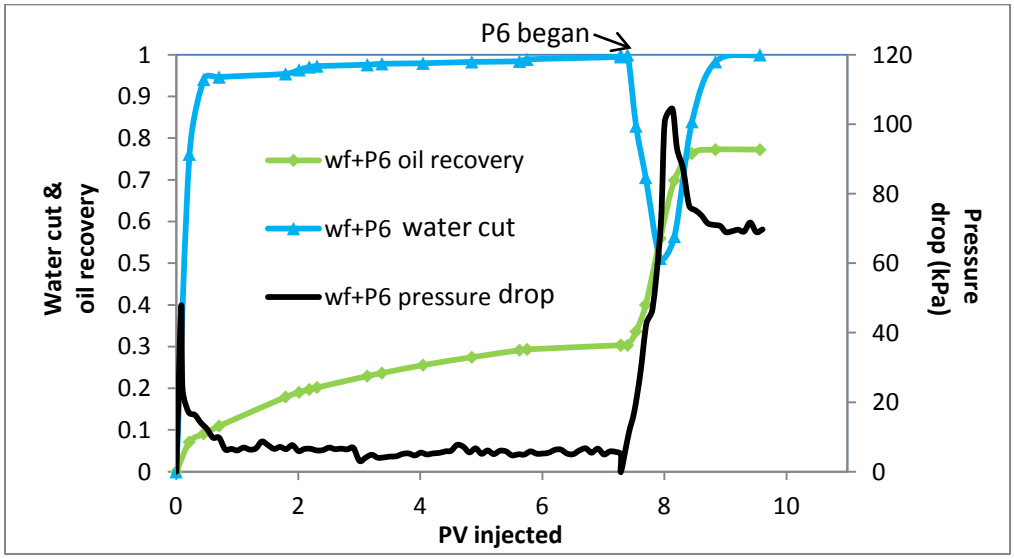

Figure 4-8: Summary of recovery, pressure drop and water cut for Displacement #2

For Displacements #1 and #2, the polymer flooding at two injection rates were conducted in the same residue oil condition, therefore the oil recovery performance can be compared,

Figure 4-9. Polymer flooding at high injection rate did not improve the oil recovery. At the relatively high IFT of the polymer displacements, the capillary number is too low to mobilize residual oil to water at any flow rate. Also, any improvement in oil mobilization due to higher velocity (and therefore higher capillary number) may be counteracted by lower sweep efficiency at high flow rates. This phenomenon was observed by Asghari et al (2008). They concluded that for the polymer flooding, at the range of concentration from 0 to 10000 ppm, within the injection rate ranging from 0.01 m/hr to 0.64 m/hr, high injection rate cannot improve the heavy oil recovery in the sandpack with permeability of 2.1 to 13.0 Darcy. They attributed this lack of improvement to higher viscous fingering at higher injection rates. Note, the viscous fingering effects would be observed at moderate oil recoveries but are not likely a factor in the ultimate recovery particularly when it nears 80%. This recovery factor is almost certainly set by the displacement efficiency.

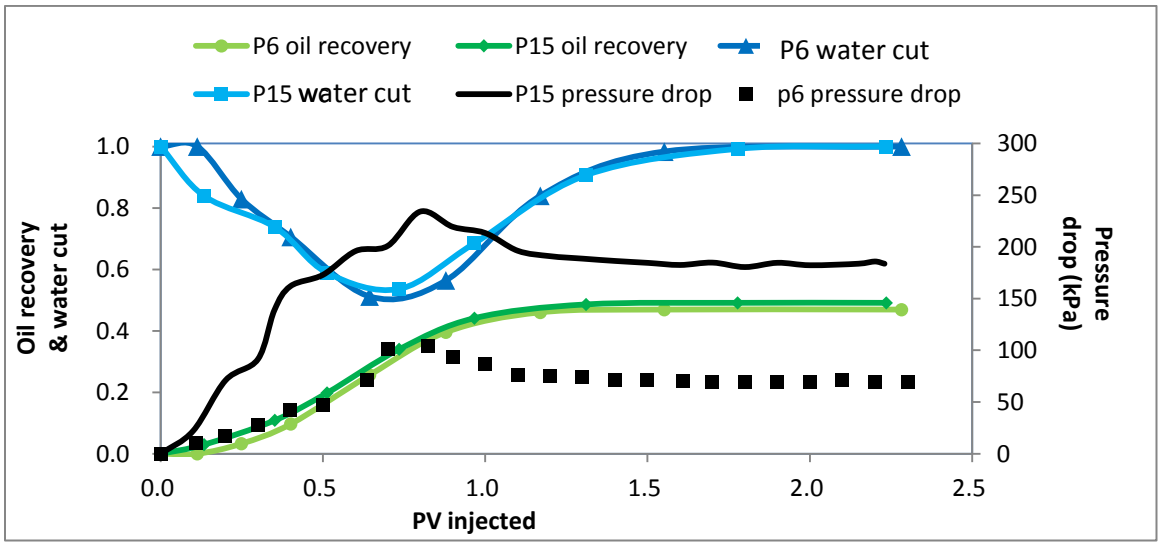

Figure 4-9: Comparison of polymer floods at 6 and 15 cm ³/hr.

4.5.3 Water Flooding at 15cm ³/hr and ASP Flooding at 15cm ³/hr

The next two displacement tests (Displacement #3 and #4) were designed to compare ASP with polymer flooding and to determine if alkali and surfactant contribute to extra oil recovery. Sandpack# 3 was conducted as water flooding and alkali-surfactant-polymer

flooding both at 15 cm³/hr. The viscosity ratio between ASP solution and oil was 0.21 approximately half that of the ratio for polymer and oil. The initial properties of the Sandpack# 3 after the oil flooding are presented in Table 4-7. Similarly to the previous displacement tests, 7.1 PV of brine were injected until the water cut approached 100% and the oil production recovery reached 27.1% of OOIP, Figure 4-10.

Table 4-7: Initial condition of Sandpack# 3 after oil flooding

Porosity (%)	35.4
Permeability (D)	6.01
OOIP (cm^3)	48.33
Oil saturation (%)	73.9
Irreducible water saturation (%)	26.1
Oil viscosity (Pa.s)	497
Oil density (g/cm^3)	0.9418

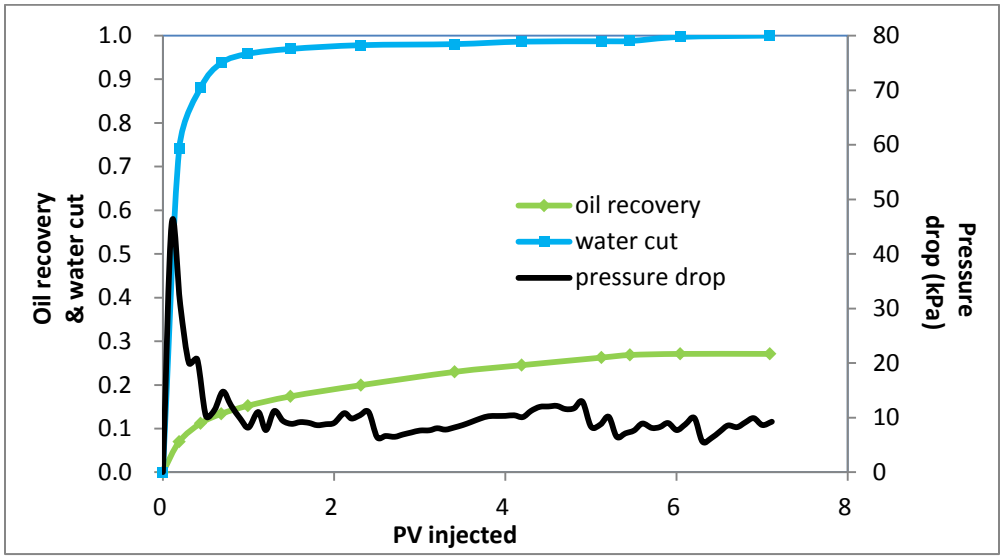

Figure 4-10: Oil recovery, water cut and pressure drop during water flooding of Sandpack #3

ASP flooding was conducted after water flooding and the water cut, oil recovery, and pressure drop are shown in Figure 4-11 for the ASP displacement and in Figure 4-12 for both displacements. After 1.4 PV ASP injected, the final pressure drop was steady at 71

kPa, the water cut reached 100%, and no more oil was produced. The incremental oil recovery was 51.1% of OOIP for a total recovery of 78% of OOIP.

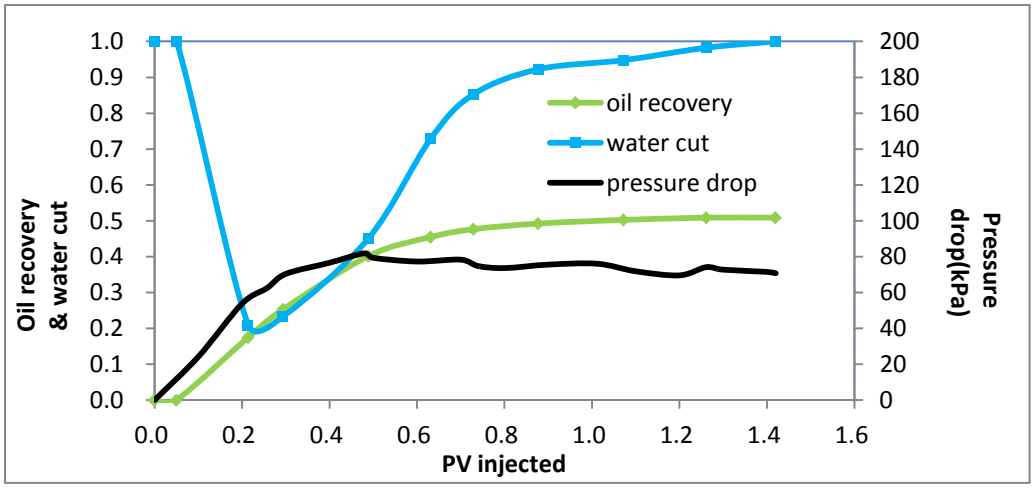

Figure 4-11: Oil recovery, water cut and pressure drop of ASP flooding at 15 cm³/hr

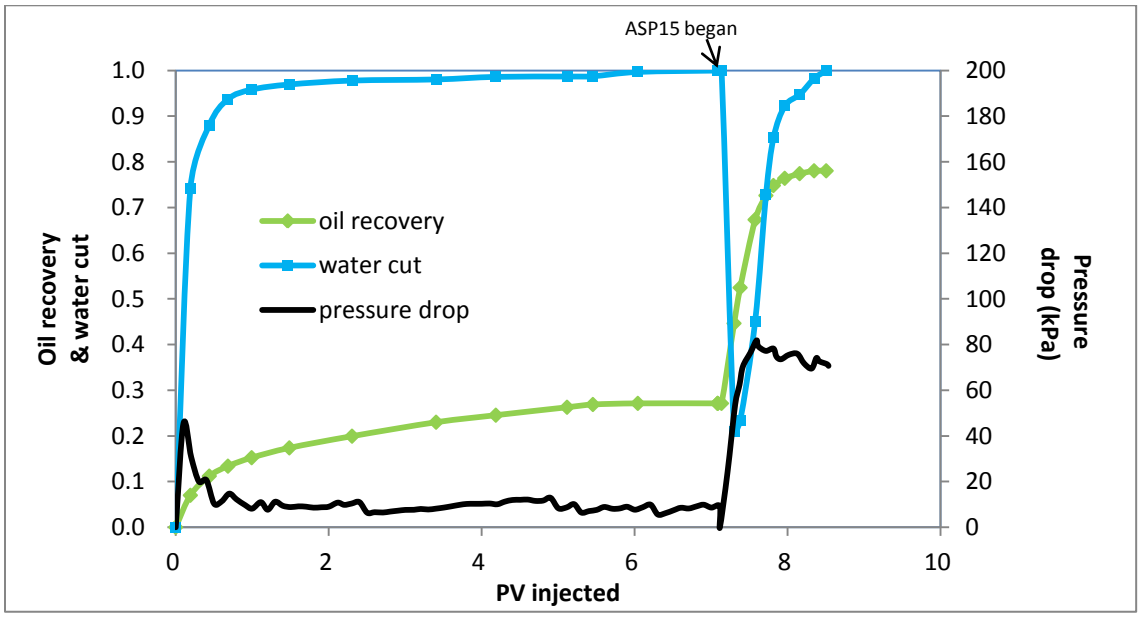

Figure 4-12: Summary of Displacement #3

Figures 4-13 and 4-14 compare the water cut, pressure drop and oil recovery of the ASP and polymer displacements at 15 cm³/hr. The incremental oil recoveries are very similar consistent with the similar end point mobility, Table 4-8. However, the interfacial tension

between ASP and oil is 0.002 mN/m compared with 8 mN/m water and polymer flooding. The substantial increase in capillary number relative to polymer is expected to increase the displacement efficiency of the ASP flood but no improvement was observed. It appears that the threshold capillary number was not reached.

The ASP flood approached the maximum incremental oil recovery at approximately half the PV injected that was required for the polymer flood. Given that the ultimate oil recoveries are similar, it seems likely that the low IFT either improves the sweep efficiency at low pore volumes of injected fluid or alters the relative permeability curves to achieve better displacement efficiency at intermediate water saturations. Also, there was substantially less pressure drop because the viscosity of the ASP was half that of the polymer. With less pore volume injection required to achieve the ultimate oil recovery and less pressure drop, the ASP displacement is the more efficient process.

Table 4-8: End point mobility comparison

M_w (water flooding before P6)	M_w (water flooding before P15)	M_2 (P6)	M_3 (P15)
0.076	0.065	0.003	0.003
M_w (water flooding before ASP6)	M_w (water flooding before ASP15)	M_2 (ASP6)	M_3 (ASP15)
0.070	0.072	0.008	0.009

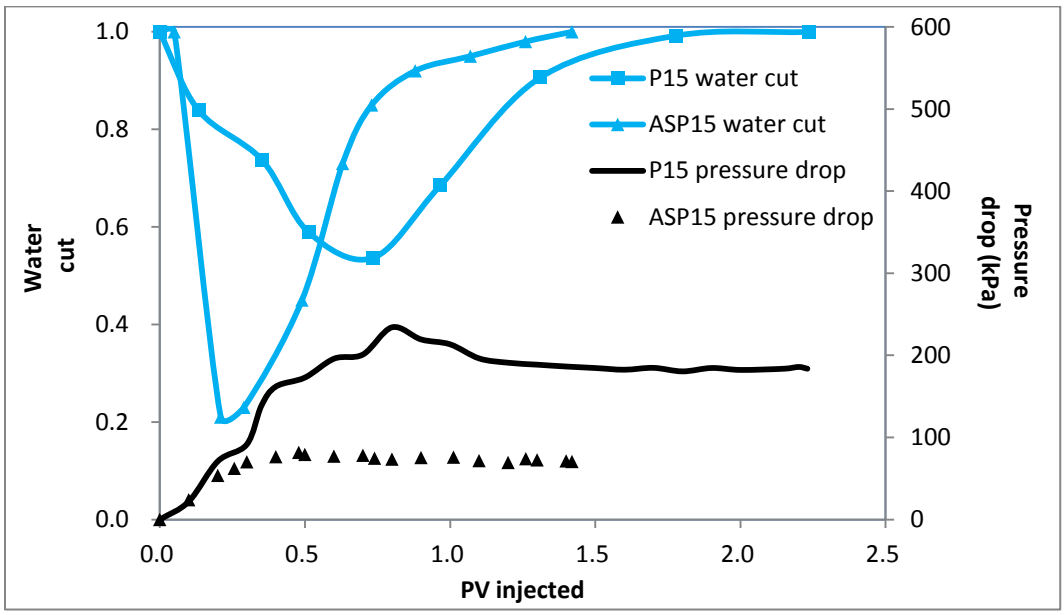

Figure 4-13: Water cut and pressure drop comparison between ASP flooding at 15 cm ³/hr and polymer flooding at 15 cm ³/hr

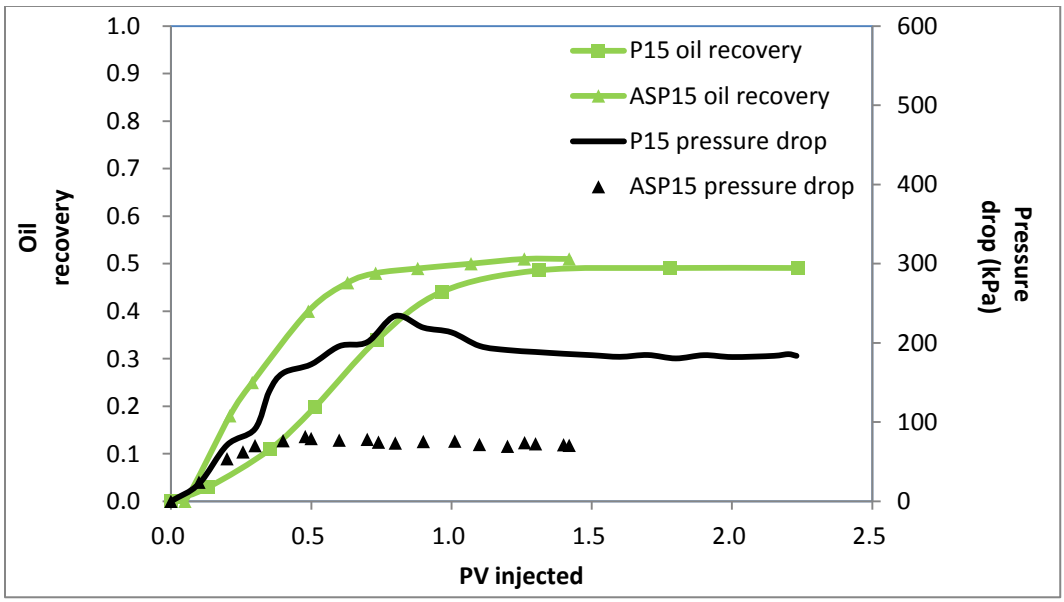

Figure 4-14: Oil recovery and pressure drop comparison for ASP flooding at 15 cm^3/hr and polymer flooding at 15 cm ³/hr

4.5.4 Water Flooding at 15cm ³/hr and ASP Flooding at 6cm ³/hr

Similarly with Displacement #3, waterflooding and ASP flooding was conducted in Sandpack #4, but ASP flooding decreased injection rate from 15 cm^3/hr to 6 cm^3/hr. The viscosity ratio of ASP solution (6 cm^3/hr) to oil was calculated to be about 0.35, which was higher than the viscosity ratio of ASP solution (15 cm^3/hr) to oil (0.21). The initial condition of the Sandpack# 4 after oil flooding is presented in Table 4-9. 7.7 PV of brine were injected until the water cut approached 100% and the oil production recovery reached 25.8% of OOIP, Figure 4-15. Subsequently, 2.3 PV of ASP was injected at a constant rate of 6cm ³/hr reached an incremental oil recovery of 62.9% of OOIP at a stabilized pressure drop of about 30 kPa, Figure 4-16. The ultimate oil recovery after water flooding and ASP flooding was 88.7%. The residual oil saturation was 8.0%.

Table 4-9: Initial condition of Sandpack# 4 after oil flooding

Porosity (%)	36.2
Permeability (D)	6.03
OOIP (cm^3)	48.33
Initial oil saturation (%)	75.2
Irreducible water saturation (%)	24.8
Oil viscosity (mPa.s)	497
Oil density (g/cm^3)	0.9418

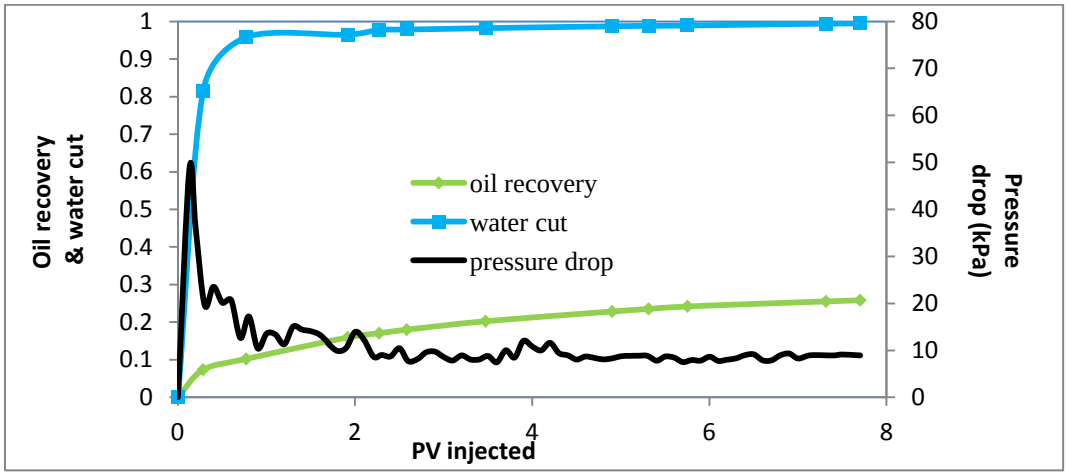

Figure 4-15: Oil recovery, water cut and pressure drop as a function of injected PV during water flooding of Sandpack #4

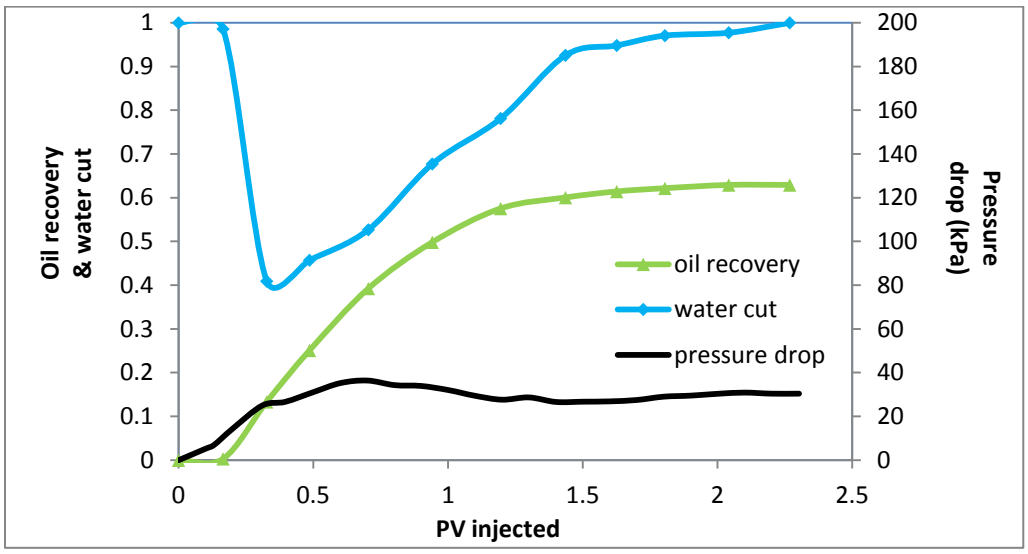

Figure 4-16: Water cut, oil recovery and pressure drop during ASP flooding at 6 cm³/hr

Figures 4-17 and 4-18 compare the water cut, pressure drop, and oil recovery between ASP flooding at the two injection rates. As expected with the lower flow rate, the pressure drop was less at 6 cm³/hr injection. The incremental oil recovery at 6 cm³/hr ASP injection was significantly greater than the oil recovery at 15 cm³/hr (63% versus 51%). The additional oil recovery appears to be related to sustained lower water cuts between 0.5 and 1.5 PV injected. However, more oil was recovered at the higher injection rate below 0.5 PV injected.

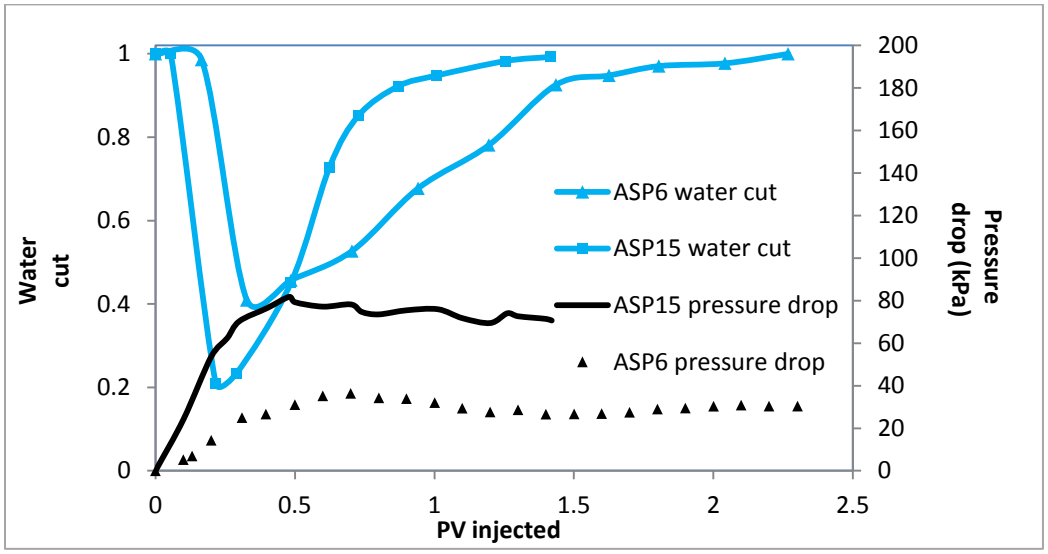

Figure 4-17: Water cut and pressure drop comparison between ASP flooding

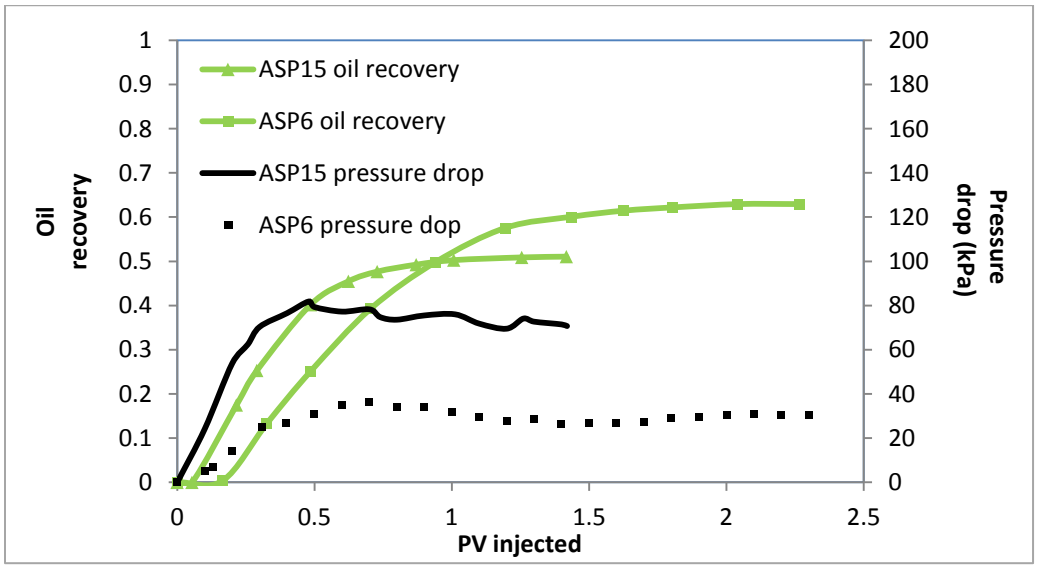

Figure 4-18: Oil recovery and pressure drop comparison between ASP flooding

The improved ultimate recovery at the lower flow rate is surprising since the capillary number will be lower and there is less chance of mobilizing the residual oil to water. The difference is not likely a result of differing sweep efficiencies (e.g. viscous fingering) because the ultimate recoveries exceed 80% in both cases and the final water cuts approach 100%. In fact, the 15 cm^3/hr injection cases recovers more oil at less than 1 PV

injected than the 6 cm³/hr case suggesting better sweep efficiency at the higher injection rate. Note that both cases provided similar end point mobilities, Table 4-8.

The difference in ultimate recovery may depend how much surfactant reaches the water-oil interface. The surfactant concentration depends on the balance of diffusion from the displacement fluid and adsorption losses to the rock surface throughout the core. Hence, the local concentration may vary and so will the ability to mobilize the residual oil. Perhaps the low flow rate allows more surfactant to diffuse to the water-oil interface in less accessible pores so that more residual oil is mobilized.

Figures 4-19 to 4-20 show that, as with the 15 cm³/hr case, the 6 cm³/hr ASP flood produced more oil at a given PV injected than the polymer flood and with less pressure drop. Hence, the ASP flood is a more efficient process. It may be possible to optimize the process further with appropriate selection of flow rates and solution viscosity.

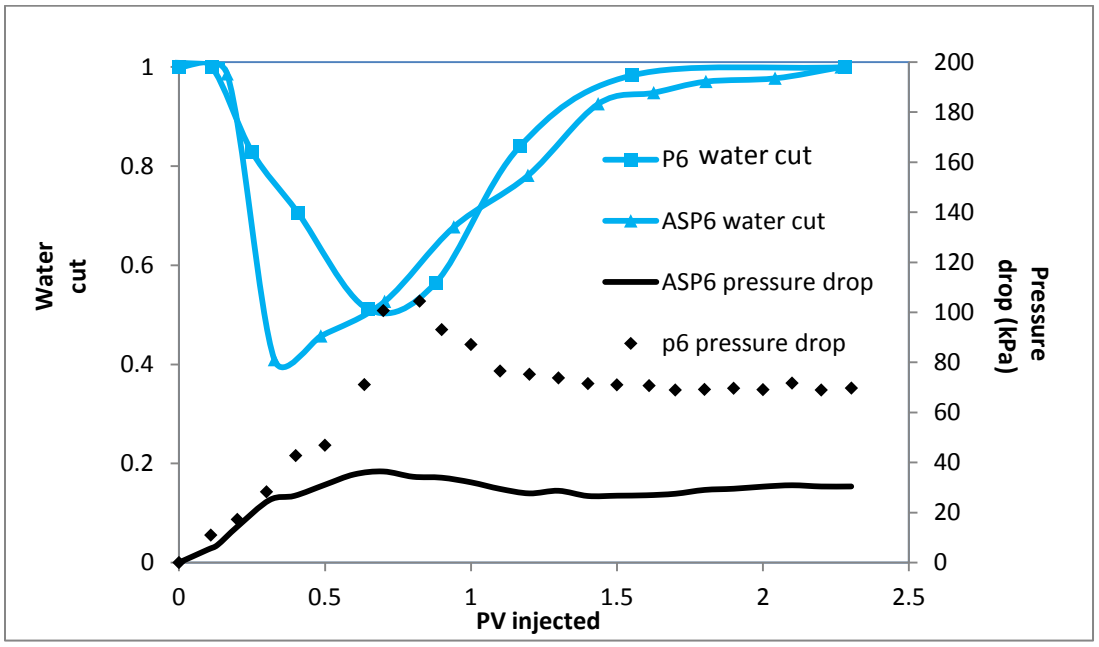

Figure 4-19: Water cut and pressure drop comparison between ASP flooding at 6 cm^3/hr and polymer flooding at 6 cm^3/hr

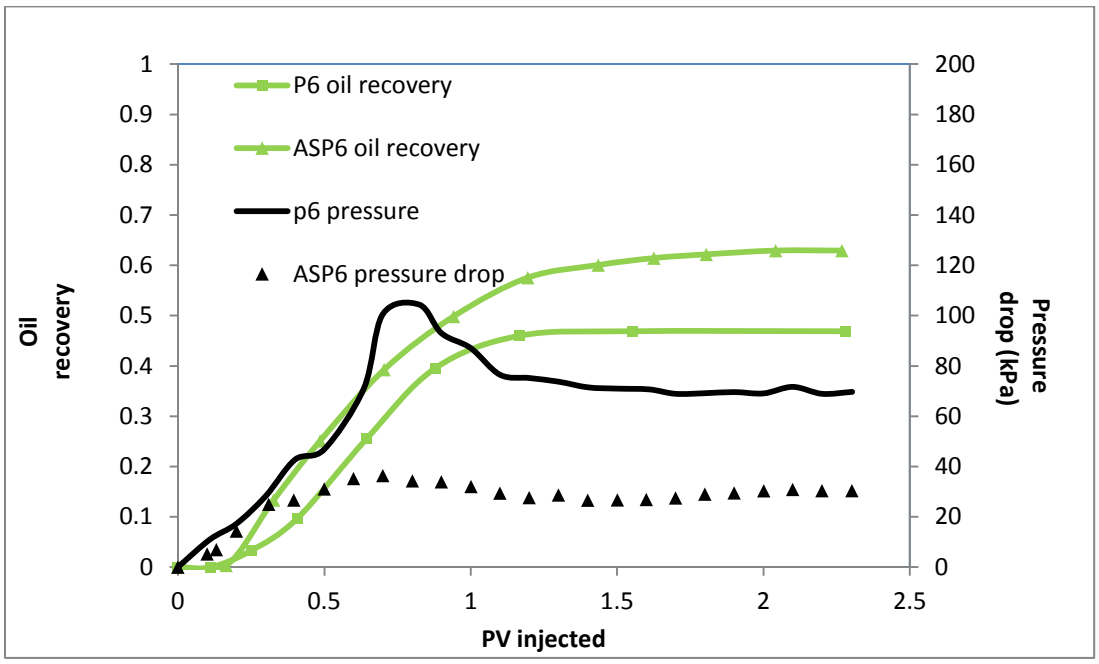

Figure 4-20: Oil recovery and pressure drop comparison between ASP flooding at 6 cm^3/hr and polymer flooding at 6 cm^3/hr

4.5.5 Water Flooding at 15 cm^3/hr and ASPF Flooding at 15 cm^3/hr

Sandpack# 5 was conducted as a sequence of water flooding and ASPF flooding. The oil recovery performance of ASPF will be compared with ASP flooding in Displacement #1. The only difference between Displacement#5 and #1 was the added gas (Nitrogen). The initial condition of the Sandpack#5 after oil flooding is presented in Table 4-10. The oil recovery from water flooding was 30.7% of OOIP, Figure 4-21.

Table 4-10: Initial condition of the Sandpack# 5 after oil flooding

Porosity (%)	36.9
Permeability (D)	5.55
OOIP (cm^3)	53.75
Initial oil saturation (%)	76.0
Irreducible water saturation (%)	24.0
Oil viscosity (mPa.s)	497
Oil density (g/cm^3)	0.9418

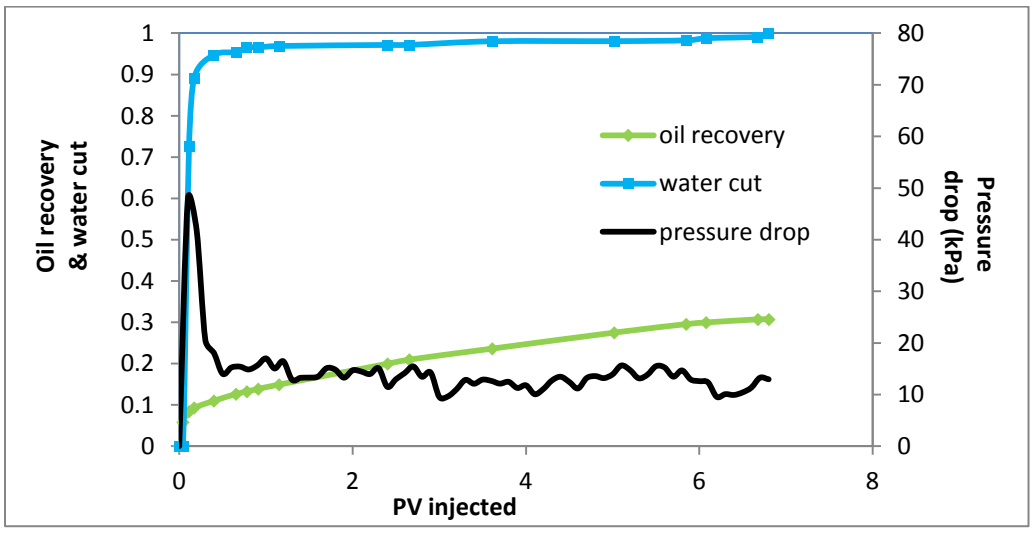

Figure 4-21: Oil recovery, water cut and pressure drop as a function of PV injected during water flooding of Sandpack #5

During ASP foam flooding, 9.69 PV of foam was injected at a rate of 15 cm^3/hr with 80% foam quality (liquid injection rate: 3cm^3/hr, gas injection rate: 12 cm^3/hr), until the oil production was close to zero, Figure 4-22. Note that 9.69 PV of foam only contained 1.94 PV of liquid ASP solution. Figure 4-23 summarizes the water cut, pressure drop and oil recovery for the waterflood and foam flood combined. The pressure drop stabilized at approximately 75 kPa, the water cut approached 100%, and 50.9% OOIP was recovered after 9.69 PV of foam injection. The ultimate oil recovery for water flooding and foam flooding was 80.6%. The residual oil saturation was 15.0%. The performance of the ASPF flood was similar to the ASP flood, Figures 4-24 and 4-25. In fact, the ASPF flood required more PV injected to achieve the same recovery. Hence, the foam did not improve recovery and made the process less efficient. Possible explanations are discussed in the next section.

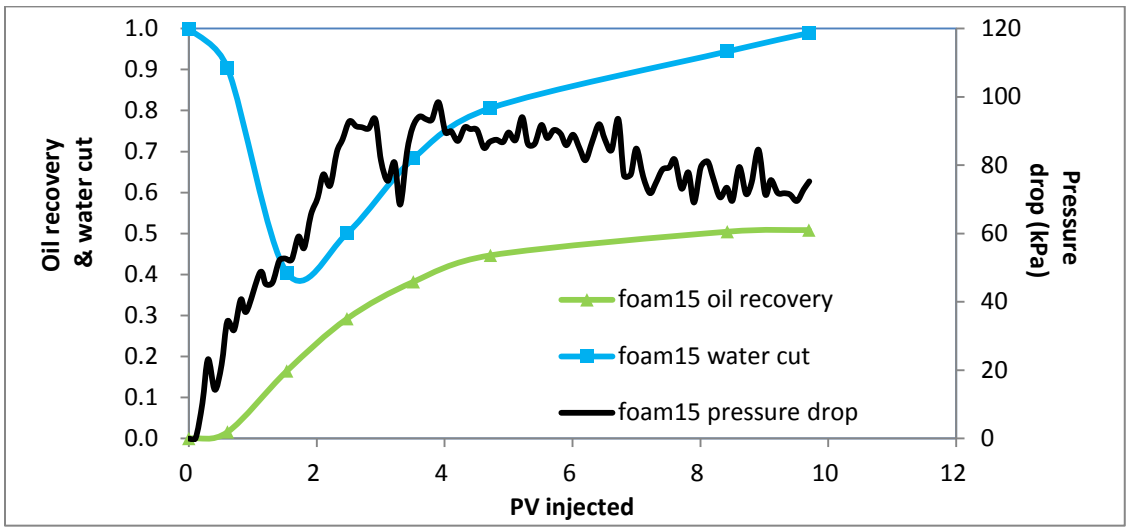

Figure 4-22: Water cut, oil recovery and pressure drop as a function of PV injected during foam flooding at 15 cm ³/hr

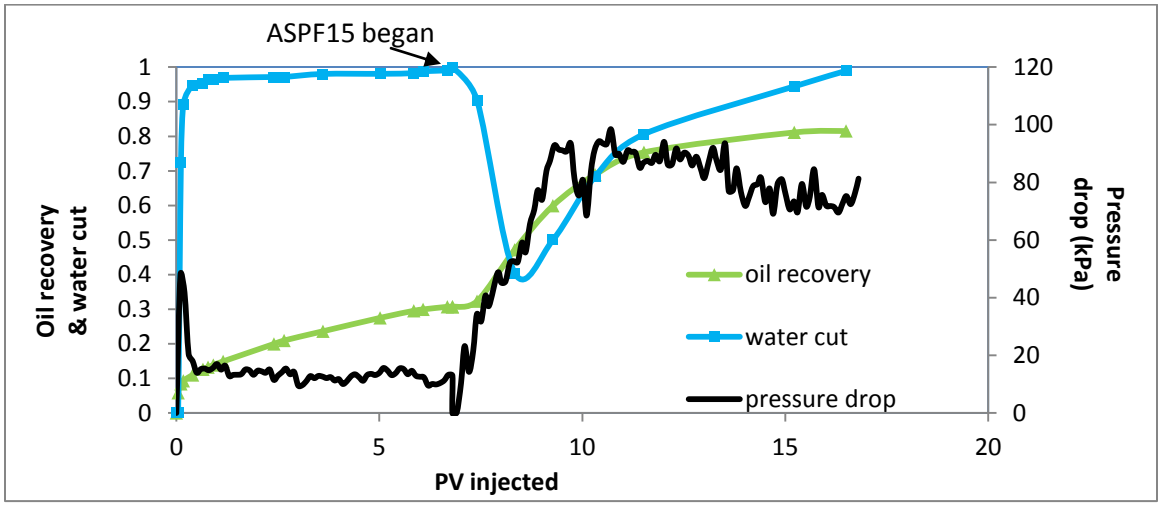

Figure 4-23: Summary of Displacement #5

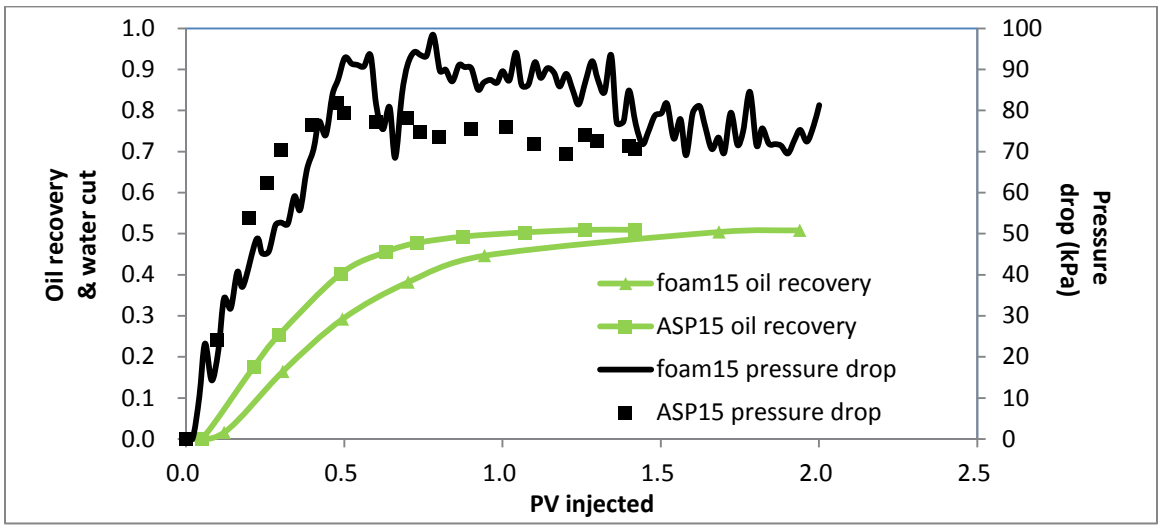

Figure 4-24: Oil recovery and pressure drop comparison between ASPF flooding and ASP flooding as a function of injected PV of liquid solution

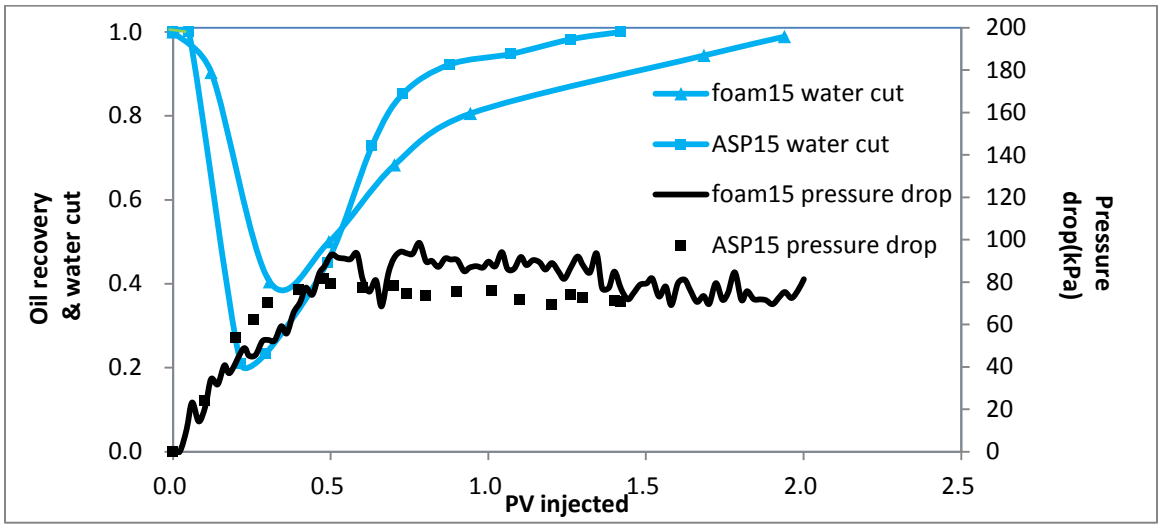

Figure 4-25: Water cut and pressure drop comparison between ASPF flooding and ASP flooding as a function of injected PV of liquid solution

c

4.5.6 ASP Foam Flooding at 15 cm^3/hr in Oil Free Condition

Sandpack# 6 was used as foam flooding in oil free condition. The displacement results will be compared with displacement #5-foam flooding in residual oil condition to study

the heavy oil effect on the foam. The initial properties of the Sandpack #6 are presented in Table 4-11.

Table 4-11: Initial condition of Sandpack# 6 after saturating with brine.

Porosity (%)	36.3
Permeability (D)	5.69
OOIP (cm^3)	N/A
Oil saturation (%)	N/A
Irreducible water saturation (%)	N/A

The brine saturated sandpack was then flooded with 2.5 PV of ASP foam injection. The pressure drop across the core also increased significantly as the ASP saturation increased as expected for the more viscous fluid and eventually stabilized at 110 kPa, Figure 4-26. The water and gas saturations were determined from material balance and are also shown on Figure 4-26. The final water saturation was approximately 25%. In other words, in this oil-free sandpack, 75% of the liquid in the porous medium was swept by the foam.

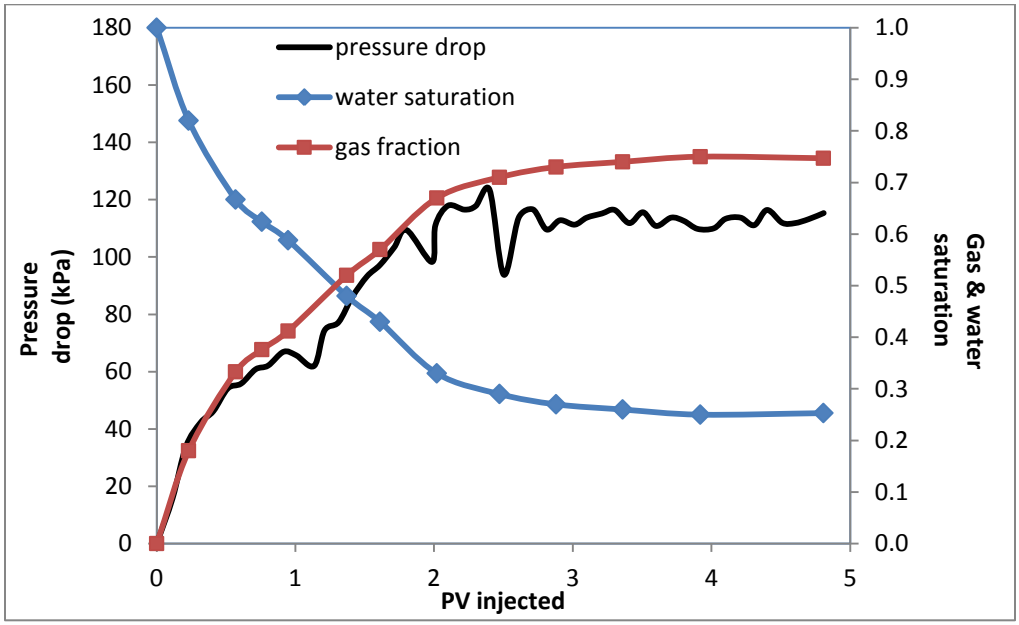

Figure 4-26: Gas, water saturation and pressure drop as a function of injected PV

During ASP foam flooding, CT scans were performed and saturation profiles and average saturations within the sandpack were determined. The average satuarations from the CT analysis were in good agreement with the material balance calculations, Table 4-12. The saturation profiles are provided in Figure 4-27.

Table 4-12: Comparison of water saturation between mass balance calculation and CT analysis

Mass balance		CT data analysis	
s_w	PV injected	s_w	PV injected
1	0	1	0
0.667	0.57	0.688	0.57
0.624	0.76	0.628	0.76
0.588	0.95	0.564	0.95
0.276	2.47	0.264	2.47
0.253	4.80	0.231	4.80

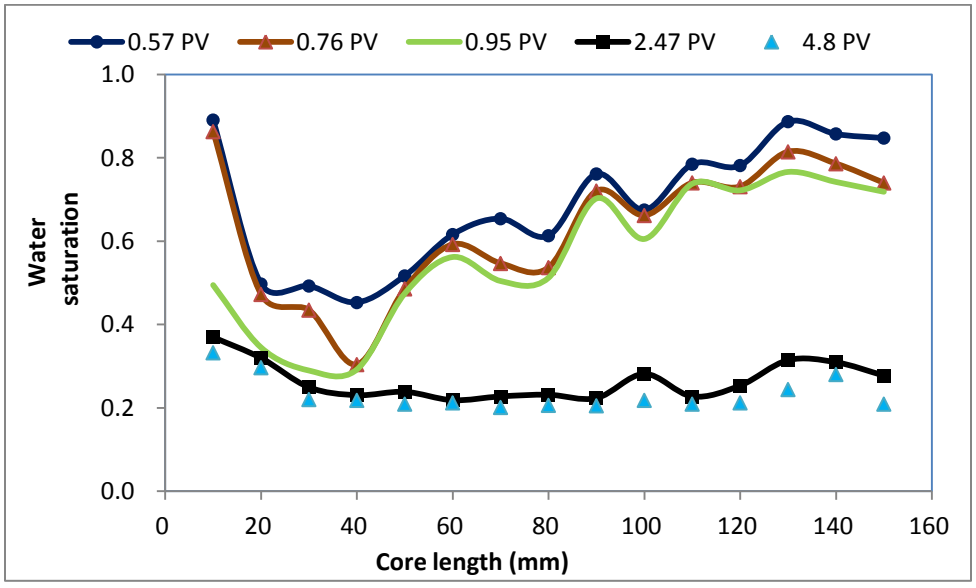

Figure 4-27: Water saturation distribution as a function of time (CT analysis)

The first CT scan was performed after 0.57 PV of foam injection and foam had already broken through at this point. Below 2.5 PV injected, the water saturation near the inlet

remained high suggesting that the foam was not evenly distributed at the inlet. Comparing the 0.95 PV profile with the 0.57 profile, it appears that the foam formed a bank that gradually sweeps through the core. It is not clear why there was such a significant change in sweep between the 0.95 PV and 2.47 PV profiles. Little additional sweep was obtained after 2.47 PV injected.

In order to determine the differences between foam flooding in oil-saturated and oil-free condition, the pressure drop during two foam flooding processes are compared in Figure 4-28. The pressure drop in the oil-free sandpack increased more than in the oil-saturated sandpack. Also more PV injected were required to reach a steady state. The longer stabilization time and lower pressure drop suggest that the foam was destroyed in the presence of heavy oil. After foam was broken, gas could channel through the oil containing area and no additional recovery was obtained from the foam.

Note that pressure drop fluctuated during foam flooding in oil condition while pressure curve was smooth in oil free condition. This was probably because foam was fragile in the presence of oil. The foam likely broke in the sandpack causing a decrease in the pressure drop. At the same time, newly injected foam gathered in the sandpack and increased pressure drop leading to pressure drop fluctuations.

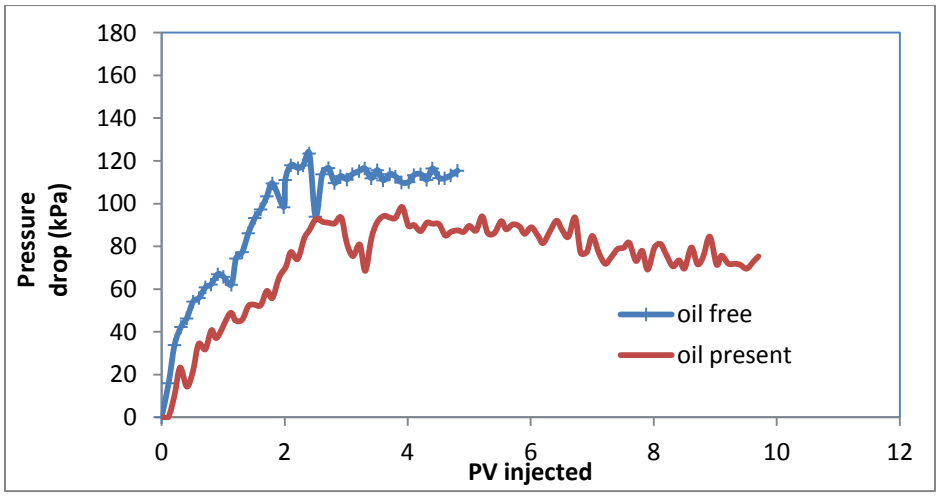

Figure 4-28: Comparison of pressure drop during foam flooding in oil and oil free condition

4.5.7 Displacement Summary

The recovery factors for all of the displacement tests are summarized in Table 4-13. The average recovery factor after waterflood was 29%. The incremental recovery from polymer, ASP, and ASPF floods was approximately 50% except for ASP at 6 cm^3/hr injection rate which provided an incremental recovery of 63%. The polymer flood recoveries were insensitive to flow rate. The ASP floods required less pressure drop and recovered more oil at lower PV injected and therefore are more efficient processes.

The ASP flood at 6 cm^3/hr likely displaced more oil because the surfactant reduced IFT sufficiently to mobilize residual oil to water. It is not clear why this oil was not mobilized at the higher flow rate but it seems that insufficient surfactant reached the water-oil interface in the pores containing the residual oil.

Table 4-13: Recovery summary of displacement tests

	Polymer (15cm^3/hr)	Polymer (6cm^3/hr)	ASP (15cm^3/hr)	ASP (6cm^3/hr)	ASP foam (15cm^3/hr)	ASP foam (no oil)
Water flooding oil recovery (%)	29.8	30.3	27.1	25.8	30.7	-
Tertiary oil recovery (%)	49.1	46.9	51.1	62.9	50.9	-
Ultimate oil recovery (%)	78.9	77.2	78.2	88.7	80.6	-
Pressure drop during steady state (kPa)	183	69	71	30	75	114

Chapter Five: CONCLUSIONS

For water flooding, water had breakthrough very early, which indicated a poor recovery before water breakthrough. And most of oil came from after water breakthrough. This indicated the significance of post breakthrough stage.

Foam flooding had a very similar oil recovery as ASP did. The performance of foam in oil free conditions indicated its blocking and diverting capacity. In addition, by comparing foam displacement performance in oil and oil free conditions, we can conclude that foam was vulnerable in the presence of heavy oil. After foam was broken, gas could channel through the oil containing area. Besides, based on the displacement comparison between ASP foam and ASP, we can find that it was ASP solution instead of foam that improved the oil recovery.

Oil recovery of polymer flooding was satisfactory, which was because of improvement of viscosity ratio between displacing solution to oil. In addition, end point mobility indicated that there was improvement of mobility after polymer was added into the displacement solution.

Under the same injection rate, comparing with the viscosity of polymer solution, the viscosity of ASP solution was lower. However, ASP showed the same or even more oil recovery comparing with polymer flooding and foam flooding, which can contribute to its improvement of displacement efficiency and sweep efficiency.

Research on the effect of injection rate indicated that ASP at 6 cm^3/hr had a better performance in oil recovery, comparing with ASP at 15 cm^3/hr. The difference in ultimate recovery may depend how much surfactant reached the water-oil interface. Besides, in high injection rate, shear thinning properties decreased the viscosity of ASP solution. For Polymer flooding, there was no apparent change of oil recovery between 6

cm^3/hr and 15 cm^3/hr, this was probably because improvement in oil mobilization due to higher velocity was counteracted by lower sweep efficiency at high flow rates.

Surfactant products Petrostep C-1 and C-2 were tested on the basis of Ross-Miles method and surface tension measurement. By comparison between these two products, Petrostep C-1 was chosen for ASP and ASP-foam displacement tests. Based on the interfacial tension measurements, IFT between ASP solution and heavy oil can reach 0.002 mN/m, comparing with more 8 mN/m between water and heavy oil. However, in the presence of heavy oil, this surfactant made foam vulnerable. Thus ASP-foam flooding didn't contribute extra oil recovery comparing with ASP flooding.

The addition of 0.5 wt% of sodium carbonate to the base solution (brine) significantly decreased the IFT between water solution and heavy oil (from more than 8 mN/m to less than 0.08 mN/m).

Chapter Six: FUTURE WORK

1. For water flooding, water injection rate was fast, this leaded to fast oil production. However, produced water cuts reached high level immediately after small amount of water was injected, leading to inefficient oil recovery. In future work, it is necessary to do the research about water injection rates. Faster water injection can increase oil production rates, but also increase viscous fingering, thus it is necessary to optimize the injection rates. Besides, after water breakthrough, slower injection can enhance the significance of capillary force, and allow more water to access to the pores with residual oil. Thus slowing injection rate of water after breakthrough is recommended.

2. Oil with different viscosities should be investigate, artificial core in heterogeneous media like in post-CHOPS reservoirs where there are wormholes should be used for the displacement tests. To determine if the injected chemical just go through wormholes or actually access the bypassed oil in the matrix. In addition, more injection rates should be run to optimize the injection rate.

3. Running the displacement in 2D or 3D system, because high oil recovery obtained in the linear system maybe a lab artifact.

Chapter Seven: REFERENCES

Al-Muntasheri., Ghaithan A., Aramco S; Zitha P. L, and Nasr-El-Din H. A., A New Organic Gel System for Water Control: a Computed Tomography Study, SPE Journal, Volume 16, Number 1, Page 197-207, March 2010

Blaker T. Morten G. A,, Skauge A., Rasmussen L., Celius H. K., Martinsen H. A., Vassenden. F., Foam for Gas Mobility Control in the Snorre Field: The FAWAG Project. SPE 78824, presented at SPE Annual Technical Conference and Exhibition, Houston, 3-6 October, 1999

Coates, G., Xiao, L and Prammer, M., NMR Logging Principles and Applications, Halliburton Engergy Services, Texas, 1999

Dalland M. and Hanssen J., Enhanced Foams for Efficient Gas Influx Control, SPE 37217, presented at International Symposium on Oilfield Chemistry, Houston, February 1997

Dusseault M., Comparing Venezuelan and Canadian Heavy Oil and Tar Sands, SPE 2001-061, presented at the 2001 Canadian International Petroleum Conference, Calgary, June 12-14 2001

Dusseault M., University of Waterloo, waterloo, Darrell Shand, Brett Davidson, PRISM Production Technologies Inc, Pressure Pulse Workovers in Heavy Oil, SPE 79033-MS, presented at the 2002 SPE International Thermal Operations and

Heavy Oil Symposium and International Horizontal Well Technology Conference. Calgary, November 4-7 2002.

Dullien F.A.L, Porous Media: Fluid Transport and Pore Structure, Academic Press, San Diego, California, 1992

Gao S. And Gao Q., Recent progress and evaluation of ASP flooding for EOR in Daqing oil field, SPE 127714, presented at SPE EOR Conference at Oil & Gas West Asia, Muscat, April 11-13 2010

Green D.W and Willhite G.P, Enhanced Oil Recovery, Henry L. Doherty Memorial Fund of AIME, Society of Petroleum Engineers, 1998

Healy R.N., Reed R.L. and Stenmark D.G., Multiphase Microemulsion System, SPE Journal, Volume 16, Number 3, Page 147-160, June 1976

Hicks J., Paul J., Deans, Harry A., Narayanan K., Distribution of Residual Oil in Heterogeneous Carbonate Cores Using X-Ray CT, SPE Formation Evaluation, Volume 7, Number 3, Page 235-240, September 1992

Holm L.W. and Josendal V.A., Effect of Oil Composition on Miscible-Type Displacement by Carbon Dioxide, SPEJ, Page 87-98, February 1982

Jameson. C.E, the Lloydminster Heavy Oil Area, Journal of Canadian Petroleum Technology, Volume 11, Number 3, Page 17-19, July-September 1973

Kantzas A., Allsopp K, Marentette D, Utilization of Polymer Gels Polymer Enhanced Foams and Foamed Gels for Improving Reservoir Conformance, presented at Annual Technical Meeting, Calgary, June 8-11, 1997

Krumrine. P.H., Falcone J.S., and Campell T.C., Surfactant Flooding 1: The Effect of Alkali Additives on IFT, Surfactant Adsorption, and Recovery Efficiency, SPE 8998-PA, SPE Journal, Volume 22, Number 4, Page 503-513 August 1982

Krumrine P.H., Falcone J.S., and Campell T.C., Surfactant Flooding 2: The Effect of Alkali Additives on Permeability and Sweep Efficiency, SPE 9811-PA, SPE Journal, Volume 22, Number 6, Page 983-992, August 1982

Kumar M., Hoang V., and Satik C., High Mobility Ratio Water Flood Performance Prediction Challenges and New Insights; SPE 97671-PA, SPE Reservoir Evaluation & Engineering, Volume 11, Number 1, Page 186-196, February 2008

Lake L.W., Enhanced Oil Recovery, Prentice Hall Inc, January 1, 1989

Lin L, Danican S, Mueller F, A Novel Foaming Agent for Hydraulic Fracturing：Laboratory Investigation and Field Usage, presented at the 2009 SPE Eastern Regional Meeting, Charleston, September 23-25, 2009

Liu Q, Dong M, Ma S, Alkaline/Surfactant Flood Potential in Western Canadian Heavy Oil Reservoirs, presented at the 2006 SPE/DOE Symposium on Improved Oil Recovery, Tulsa, 22-26 April, 2006

Mai A. and Kantzas A., Mechanism of Heavy Oil Recovery by Low Rate Waterflooding. SPE 2008-156, presented at Canadian International Petroleum Conference, Calgary, July17-19, 2008

McClave J.T. and Sincich T, Statistics, Prentice Hall, 9th Edition, 2003

Miller K.A., Improving the State of the Art of Western Canadian Heavy Oil Waterflood Technology, Journal of Canadian Petroleum Technology, Volume. 45, Number. 4, April 2006

Miller K. A., State of the of Western Canadian Heavy Oil Waterflood Technology, PETSOC-2005-251-P, presented at Canadian International Petroleum Conference, Calgary, June 7-9, 2005

Morriss. C, Rossini D, Straley C, Tutunjian P, Vinegar H, Core Analysis by Low-field NMR, The Log Analyst, Volume 38, Number 2, March-April, 1997

Miao X, Gao S., Experimental study of abnormal phase behaviors of micro emulsion with Daqing oil, SPE 17840-MS, presented at International Meeting on Petroleum Engineering, 1988

Needham R. B., Doe P. H., Polymer Flooding Review, SPE 17140-PA, Journal of Petroleum Technology, Volume 39, Number 12, Page 1503-1507, December 1987

Qu Z., Zhang Y., Zhang X., Dai. J., A Successful ASP flooding Pilot in Gudong Oil Field, SPE 39613-MS, presented at SPE/DOE Improved Oil Recovery Symposium, Tulsa, April 19-22, 1998

Rojas Y, Kakadjian S, Aponte A, Marquez R, Sanchez G, PDVSA-Intevep, Stability and Rheological Behavior of Aqueous Foams for Underbalanced Drilling, presented at SPE International Symposium on Oilfield Chemistry, Houston, February 13-16, 2001

Rosen S. L., Fundamental Principles of Polymeric Materials, Wiley-lnterscience Biomaterials, Volume 3, Issue 4, Page 253, October 1982

Salama. D, Kantzas. An Experimental Observations of Miscible Displacement of Heavy Oils with Hydrocarbon Solvents, SPE 97854-MS, presented at SPE/PS-CIM/CHOA International Thermal Operations and Heavy Oil Symposium, Calgary, November 1-3, 2005

Sydansk R.D, Polymer-Enhanced Foam Propagation through High Permeability Sandpack. SPE 25175, presented at the SPE International Symposium of Oilfield Chemistry, New Orleans, March 2-5, 1993

Taber J.J, Dynamic and static forves required to remove a discontinuous oil phase from porous media containing both oil and water, SPEJ, Page 3-12, March, 1969

Veil J.A., Quinn J.J., and Garcia J.P., Water Issues Relating to Heavy Oil Production, SPE 120630-MS, presented at SPE Americas E&P Environmental and Safety Conference, San Antonio, March 23-25, 2009

Wang D, Cheng J, Yang Z, Li Q, Wu W and Yu H, Successful Field Test of the First Ultra-Low Interfacial Tension Foam Flood, SPE72147-MS, presented at SPE Asia Pacific Improved Oil Recovery Conference, Kuala Lumpur, October 6-9, 2001

Wang D, Xia H, Wang Y, Liu Z and Yang Q, Study of the Mechanism of Polymer Solution with Visco-Elastic Behavior Increasing Microscopic Oil Displacement Efficiency and the Forming of Steady "Oil Thread" Flow Channels, SPE 68723, presented at SPE Asia Pacific Oil and Gas Conference and Exhibition, Jakarta, April 17-19, 2001

Wassmuth F.R, Hodgins L.H, Schramm L.L, Kutay. S.M., Screening and Coreflood Testing of Gel foams to Control Excessive Gas Produciton in Oil Wells, SPE 59283, presented at the 2000 SPE/DOE Improved Oil Recovery Symposium, Tulsa, April 3-5, 2000

Wellington S.L., SPE, and H.J. Vinegar, X-Ray Computerized Tomography, SPE 16983-PA, Journal of Petroleum Technology, Volume 39, Number 8, Page 885-898, August 1987

Zhang Y. P., Dong M., Determining the Most Profitable ASP Flood Strategy for Enhanced Oil Recovery, SPE 2003-015 presented at Canadian International Petroleum Conference, Calgary, Jun 10 - 12, 2003

Zhang Y., Yue X., Dong J., Yu L., New and Effective Foam flooding to Recover Oil in Heterogeneous Reservoir., SPE 59367 presented at the 2000 SPE/DOE improved Oil Revovery Symposium, Tulsa, Oklahoma, April 3-5, 2000

APPENDIXES

Measurement of Pore Volume and Porosity

After the sandpack was prepared, its pore volume and porosity was determined by gas expansion method. Based on the Equation 3-4, we can calculate the pore volume and porosity. The porosity can be measured within $\pm 0.1\%$. Three measurements of porosity were conducted for each sandpack to ensure the repeatability, which was $\pm 1.7\%$ based on 90% confidence interval.

Table 8-1: Calculation of pore volume using gas expansion method

Atmosphere pressure (kPa)	88.41
Gauge pressure (kPa)	42.75
Mass of water (cm^3)	44.52
Density of water (at 25℃)	0.997
Dead volume (cm^3)	28.0
Pore volume (cm^3)	64.3
Porosity (%)	35.4

Measurement of Brine Permeability

After sandpack was saturated by brine, its permeability was determined. Table 8-2 shows the average velocity under different pressure gradients. The absolute permeability of the sandpack was determined from the slope of flow rate versus pressure gradient, as shown in Figure 8-1.

Table 8-2: Brine permeability measurements

Water height (cm)	Pressure gradient (atm/cm)	Flow rate (cm^3/min):			Average velocity (cm/s):	Permeability (Darcy)
100	0.0061	21.1	21.1	21.0	0.03	6.03
120	0.0073	26.6	26.8	26.7	0.05	
140	0.0086	32.1	32.2	32.2	0.05	

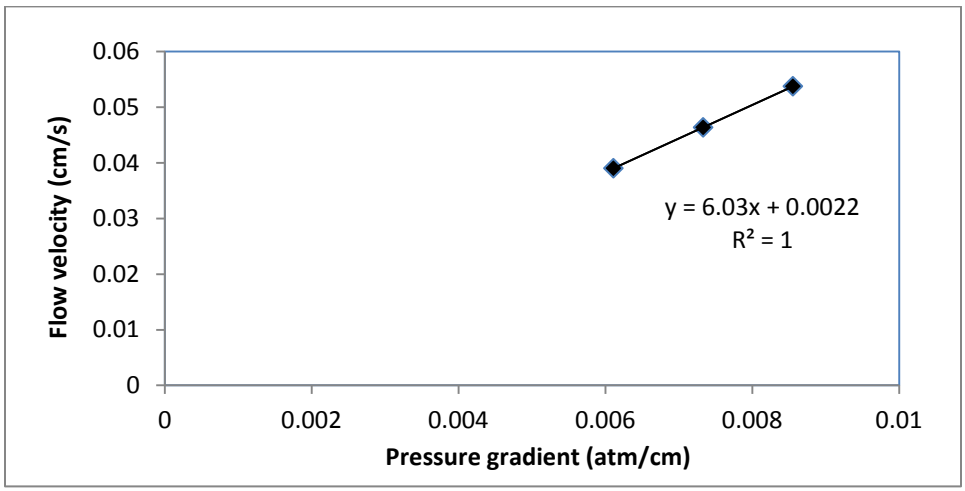

Figure 8-1: Brine permeability measurements

The permeability of all prepared sandpacks ranged from 5.55 D to 6.03 D, and Table 8-3 presented the summary of the brine permeability of the sandpacks. The permeability was capable of measuring the permeability within ± 0.01 D. Three measurements were conducted for each pressure drop to ensure the repeatability, which was ± 0.5 D based on 90% confidence interval.

Table 8-3: Summary of brine permeability

Permeability (D)	Sandpack #
5.69	1
5.55	2
6.01	3
5.69	4
6.03	5
6.01	6

Measurement of Critical Micelle Concentration (CMC)

Surface tension in different concentration of surfactant (Petrostep C1) is shown in Figure 8-2. The surface tension decreased with the increase of surfactant concentration until 4000 ppm Petrostep C1 was added. Thus 4000 ppm was Critical Micelle Concentration (CMC) of Petrostep C1.

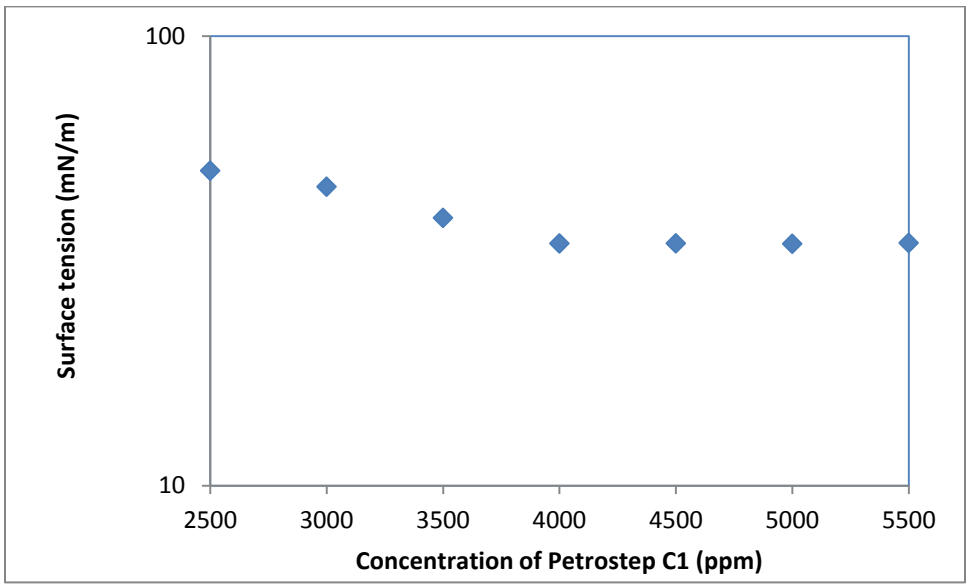

Figure 8-2: Determination of Critical Micelle Concentration

Repeatability Determination

In order to evaluate the repeatability of the measurements, 90% confidence interval was determined using the equation 8-1:

$$\overline{x} - t_{(\frac{\alpha}{2},v)}\frac{s}{\sqrt{n}} \leq \mu^* \leq \overline{x} + t_{(\frac{\alpha}{2},v)}\frac{s}{\sqrt{n}} \qquad \textbf{Equation 8-1}$$

Where $\overline{x}$ is the mean value of my measurements, μ^* is the correct mean, s is the sample standard deviation, n is the number of data points in the sample, v is the degree of freedom which is equal to n-1, and α=1-confidence interval/100. The parameter $t_{(\frac{\alpha}{2},v)}$ can be found from t-test tables (McClave and Sincich, 2003).

CT Images

By using the Kehlco imaging software provided by Kehlco Inc., the CT images for the sandpack can be output. Figure 8-3 and 8-4 shows images of Sandpack# 2 and Sandpack# 4 in dry condition. From these two figures, we can conclude that the Sandpack#2 and #4 were homogeneous. Note that no CT analysis was conducted for water flooding or

chemical flooding, because there was no density contrast between oil and water. The difference between oil and water could not be identified in the CT images.

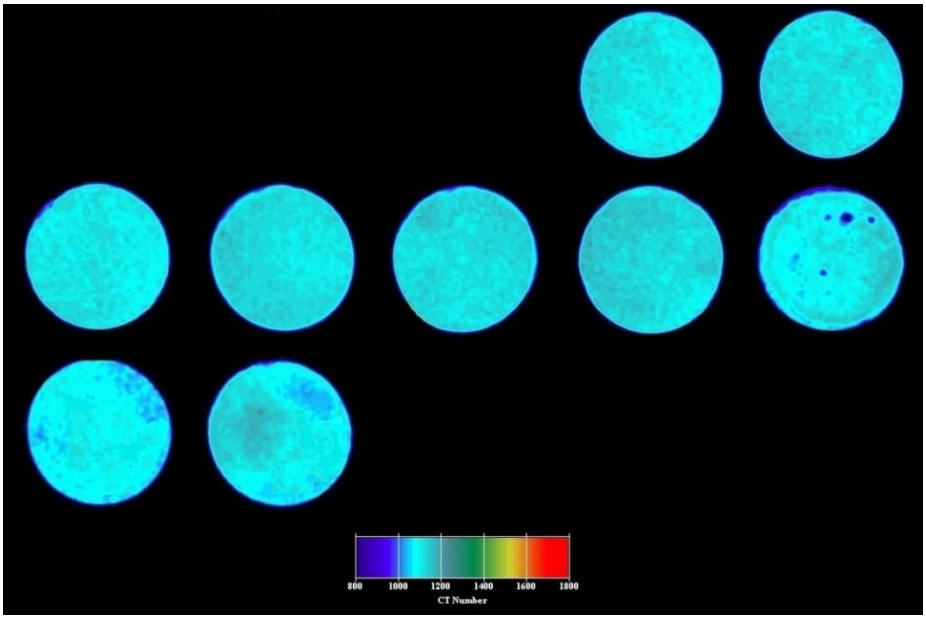

Figure 8-3: CT images of dry Sandpack #2

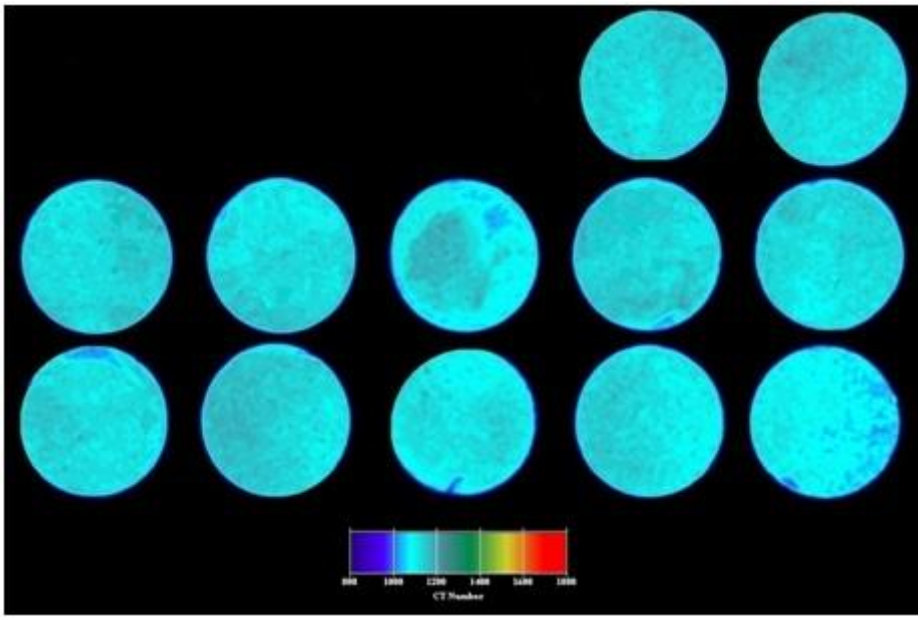

Figure 8-4: CT images of dry Sandpack #4

Figure 8-5 was about CT image of Sandpack #6 (dry core). As it shows, the sandpack was evenly packed. Note that between each image of CT scan has a 10 mm interval, first image started from 10 mm position and the last one had 150 mm position.

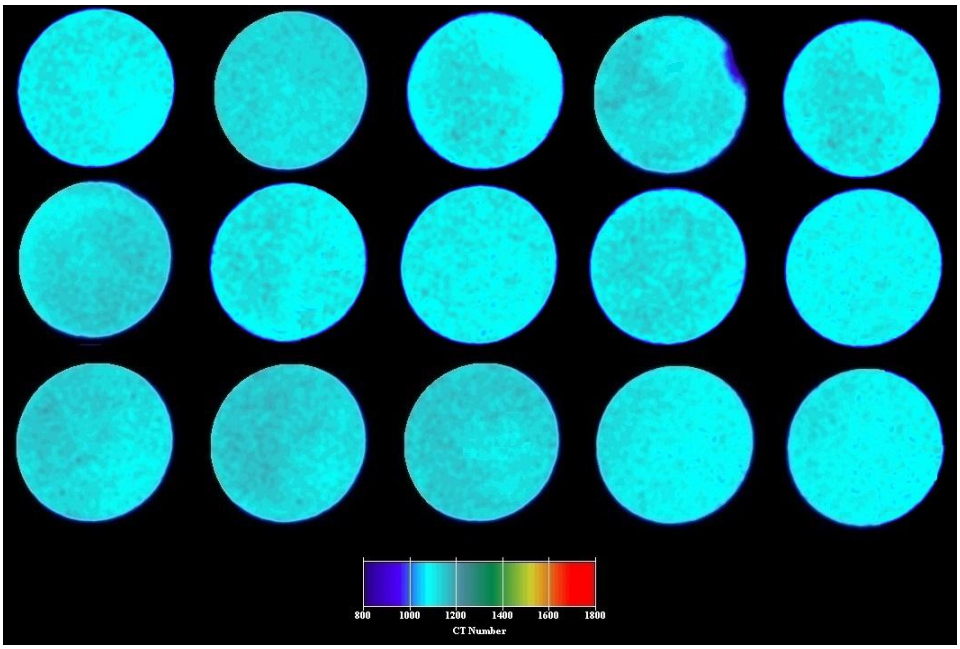

Figure 8-5: CT images of Sandpack#6 (dry core)

Figure 8-6 to 8-11 indicated how did foam performed in the porous media: The foam initially accumulated in the inlet part area. After 2.4 PV of foam was injected, the gas saturation was evenly distributed in all positions. This means new injected foam diverted into unswept area.

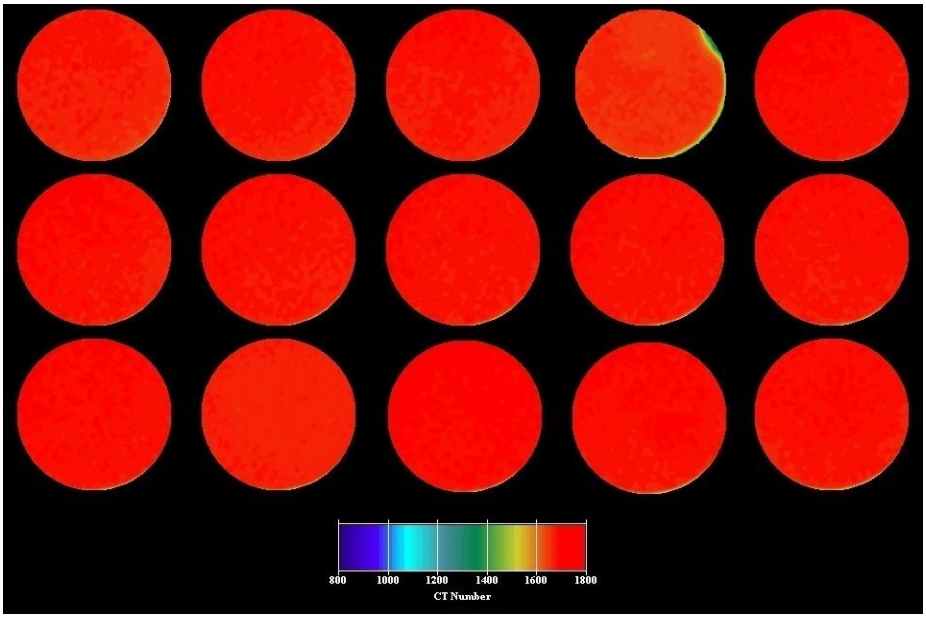

Figure 8-6: CT images of Sandpack# 6 after brine saturating

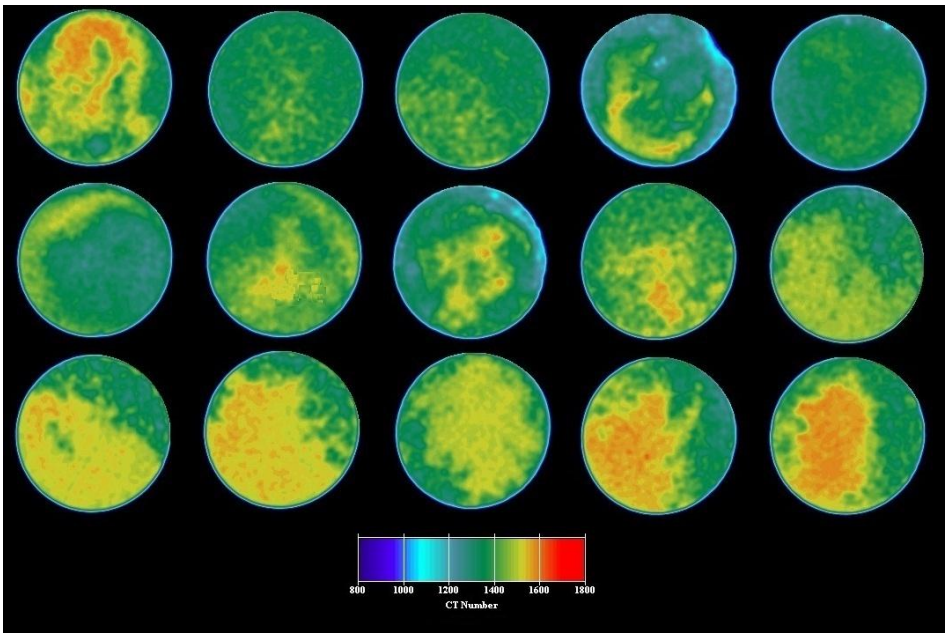

Figure 8-7: CT images of Sandpack# 6 after 0.57 PV foam was injected

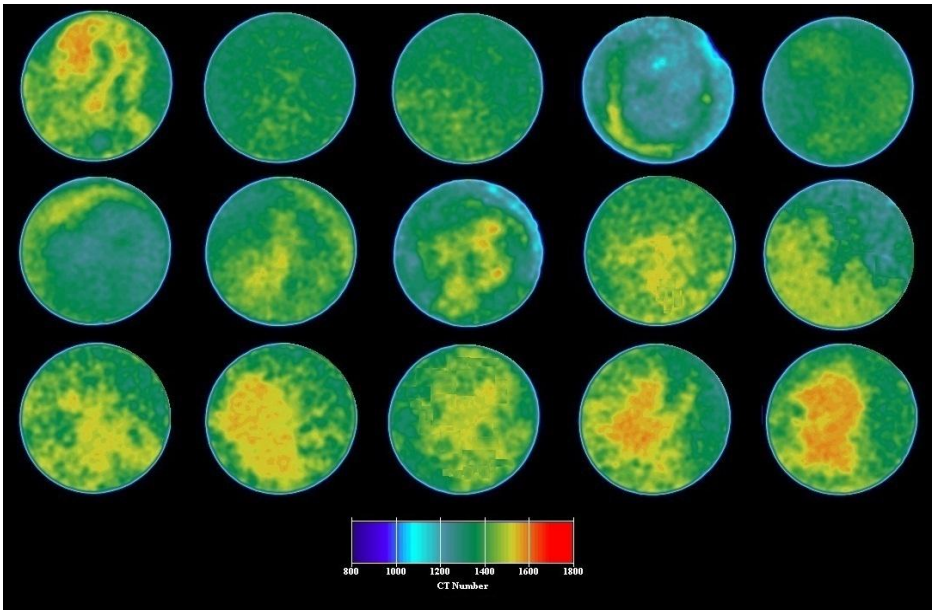

Figure 8-8: CT images of Sandpack# 6 after 0.76 PV foam was injected

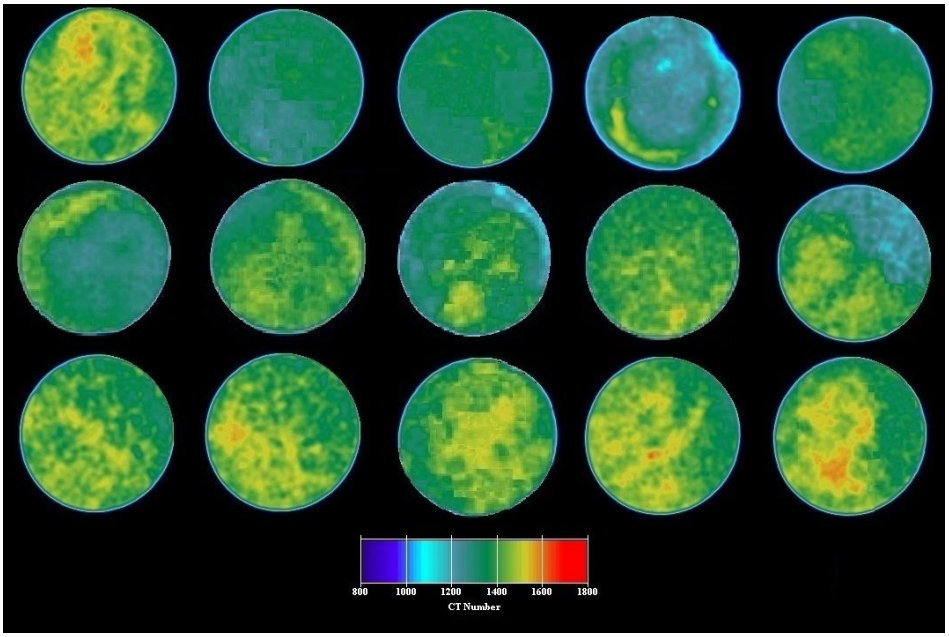

Figure 8-9: CT images of Sandpack# 6 after 0.95 PV foam was injected

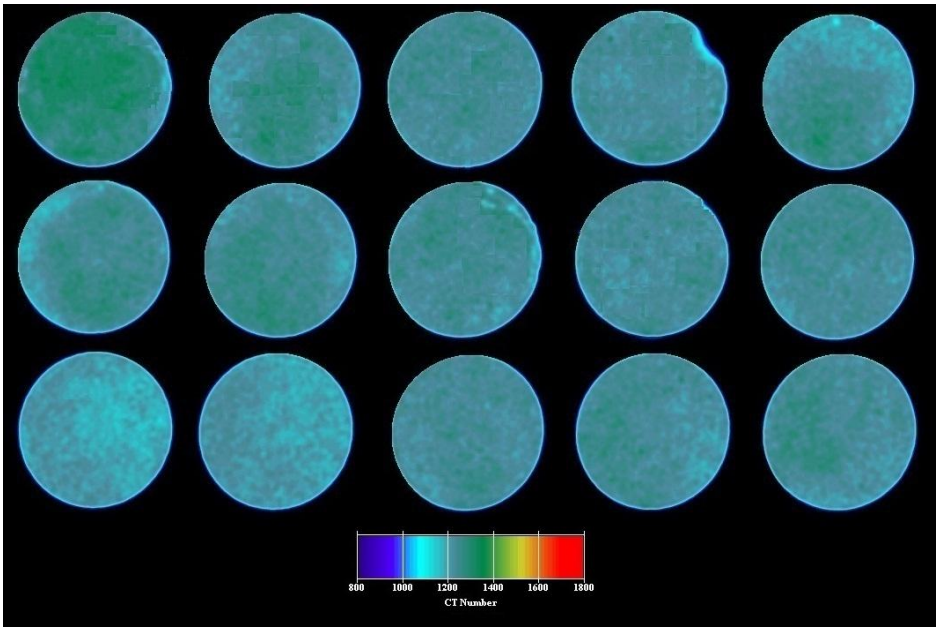

Figure 8-10: CT images of Sandpack# 6 after 2.47 PV foam was injected

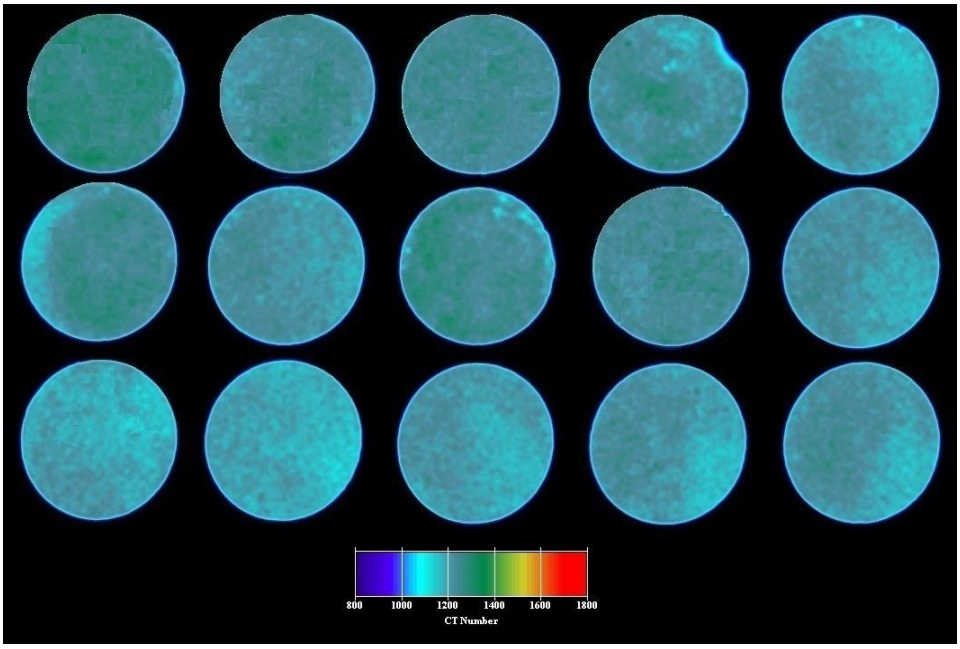

Figure 8-11: CT images of Sandpack# 6 after 4.80 PV foam was injected

For Displacement# 5, CT images of core in dry condition and post foam flooding condition can be obtained, which are shown in Figure 8-12 and 8-13. By comparing Figure 8-13 with 8-11, we can conclude that there was not much foam swept area as displacement# 6 did, which means large amount of foam could not exist in the presence of heavy oil. Foam was weak and easy to break in the presence of oil. Thus gas channelling was more severe.

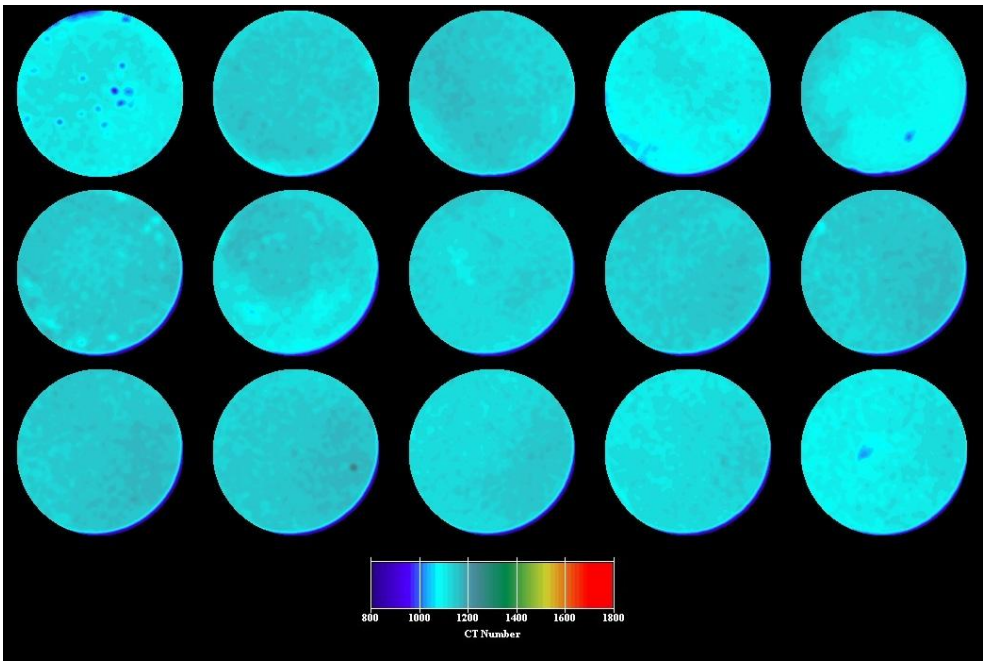

Figure 8-12: CT images of dry Sandpack #5

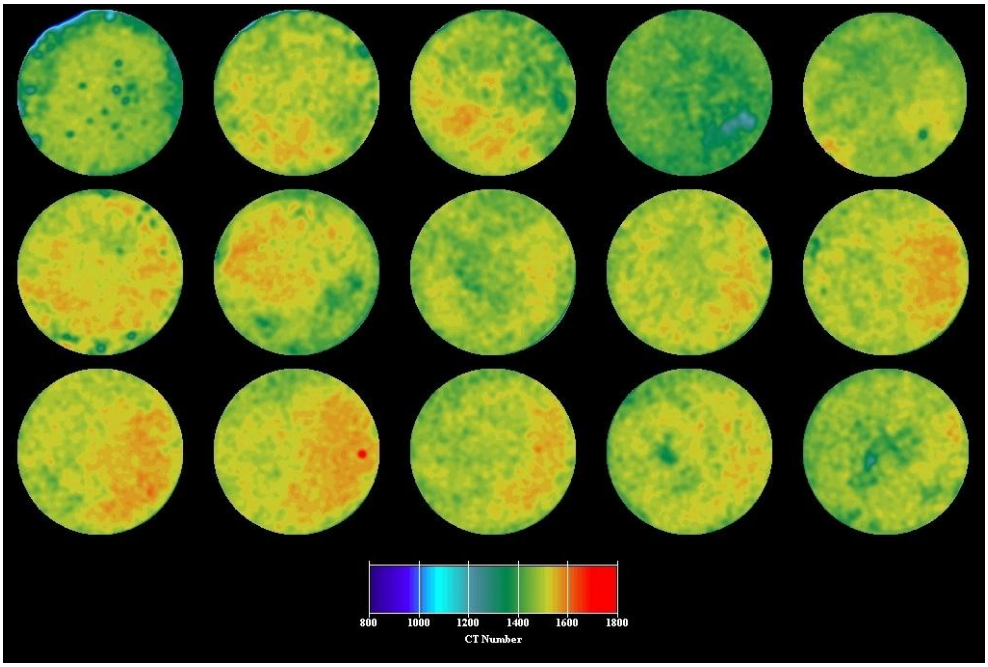

Figure 8-13: CT images of Sandpack #5 after foam flooding